AFRL-ML-TY-TR-2006-4560

DEVELOPMENT OF HIGH EFFICIENCY, LOW-COST FLEXIBLE DYE-SENSITIZED SOLAR CELLS

K. R. Thampi, Ph.D. and M. G. Graetzel, Ph.D.
Swiss Federal Institute of Technology (EPFL)
Laboratory of Photonics and Interfaces (LPI)
Institute of Molecular and Biological Chemistry (ICMB)
Lausanne, Switzerland, CH-1015

Final Report, August 2006

Air Force Research Laboratory
Materials and Manufacturing Directorate
Airbase Technologies Division
139 Barnes Drive, Suite 2
Tyndall AFB, FL 32403-5323

NOTICE AND SIGNATURE PAGE

Using Government drawings, specifications, or other data included in this document for any purpose other than Government procurement does not in any way obligate the U.S. Government. The fact that the Government formulated or supplied the drawings, specifications, or other data does not license the holder or any other person or corporation; or convey any rights or permission to manufacture, use, or sell any patented invention that may relate to them.

This report was cleared for public release by the Air Force Research Laboratory Airbase Technologies Division Public Affairs Office and is available to the general public, including foreign nationals. Copies may be obtained from the Defense Technical Information Center (DTIC) (http://www.dtic.mil).

REPORT NUMBER AFRL-ML-TY-TR-2006-4560 HAS BEEN REVIEWED AND IS APPROVED FOR PUBLICATION IN ACCORDANCE WITH THE ASSIGNED DISTRIBUTION STATEMENT.

/S/
REZA SALAVANI
Work Unit Manager

/S/
RICHARD N. VICKERS
Chief, Deployed Base Systems Branch

/S/
WENDELL D. BANKS
Chief, Airbase Technologies Division

This report is published in the interest of scientific and technical information exchange, and its publication does not constitute the Government's approval or disapproval of its ideas or findings.

REPORT DOCUMENTATION PAGE

Form Approved
OMB No. 0704-0188

PLEASE DO NOT RETURN YOUR FORM TO THE ABOVE ADDRESS.

1. REPORT DATE *(DD-MM-YYYY)*	2. REPORT TYPE	3. DATES COVERED *(From - To)*
30-08-2006	Final Technical Report	30-07-2004 - 30-08-2006

4. TITLE AND SUBTITLE

Development of High Efficiency, Low-cost Flexible Dye-sensitized Solar Cells

5a. CONTRACT NUMBER

5b. GRANT NUMBER

FA8655-03-M-13068

5c. PROGRAM ELEMENT NUMBER

62201F

6. AUTHOR(S)

Graetzel, Michael; Thampi, Ravi

5d. PROJECT NUMBER

4397

5e. TASK NUMBER

C1

5f. WORK UNIT NUMBER

4397C19C

7. PERFORMING ORGANIZATION NAME(S) AND ADDRESS(ES)

Swiss Federal Institute of Technology
Station 6
Lausanne, Switzerland, CH1015

8. PERFORMING ORGANIZATION REPORT NUMBER

9. SPONSORING/MONITORING AGENCY NAME(S) AND ADDRESS(ES)

Air Force Research Laboratory
Materials and Manufacturing Directorate
139 Barnes Drive, Suite 2
Tyndall AFB, FL 32403-5323

10. SPONSOR/MONITOR'S ACRONYM(S)

AFRL/MLQD

11. SPONSOR/MONITOR'S REPORT NUMBER(S)

AFRL-ML-TY-TR-2006-4560

12. DISTRIBUTION/AVAILABILITY STATEMENT

Distribution Statement A. Approved for public release; distribution unlimited.

13. SUPPLEMENTARY NOTES

Document contains color images.

14. ABSTRACT

This research effort focused on development of new flexible solar cells that can be integrated into deployable shelter skins for power generation purpose in remote locations. This report covers activities and results of a research program over a period of two years. The program was targeted at first realizing a molecular photovoltaic cell based on a dye sensitized nanocrystalline semi-conductor film employing a hole conductor, a conducting polymer or a polymer electrolyte reaching an AM1.5 solar-to-electric conversion efficiency of at least 10%, within the first year. This milestone was achieved within 9 months by producing solid-state solar cells containing hole conductors, with 12.56% efficiency. Further, a new type of solar cell based on polymer electrolytes was also developed in the second year. A typical cell of this type showed 12.2% solar conversion efficiency. All efficiency figures were certified by NREL, USA. In the second year, the polymer based solar cell was capable of reaching conversion efficiencies of 16.1%.

15. SUBJECT TERMS

dye sensitized nanocrystalline semiconductor, molecular photovoltaic, solar power

16. SECURITY CLASSIFICATION OF:			17. LIMITATION OF ABSTRACT	18. NUMBER OF PAGES	19a. NAME OF RESPONSIBLE PERSON
a. REPORT	b. ABSTRACT	c. THIS PAGE			Reza Salavani
U	U	U	UU	49	19b. TELEPHONE NUMBER *(Include area code)*

Reset

Standard Form 298 (Rev. 8/98)
Prescribed by ANSI Std. Z39.18

Development of high efficiency, low-cost flexible dye-sensitized solar cells

Submitted by: Prof. Michael Graetzel, Principal Investigator, Laboratory of Photonics and Interfaces, EPFL, Station 6, CH-1015 Lausanne, Switzerland
Report prepared by Dr. K.Ravindranathan Thampi, same address.

This report covers the research activity and the major findings of the USAF solar cell project for the period starting from 2004 to 2006.

1) Research Topic & Background of the research

This research topic focuses on the development of a new solar cell technology for system power applications. The Airbase Technologies division (MLQ) has a current need and investment in low-cost, flexible solar cells for power generation in their shelter structures. The Polymer Branch (MLBP) also has significant investments in organic photovoltaic technologies at the basic research level and is interested in developing related technologies. Longer-term applications cover a variety of systems including power generation for space satellite structures as well as for Air Force communication systems. The development of a low-cost and flexible solar cell with relatively high efficiency would directly impact a number of Air Force systems (current and future) and forms the basis of this research topic.

Solar cells based on organic materials is a new technology that is being developed. It differs substantially from the typical solar cell based on inorganic materials in the processing methods used. The fabrication of inorganic cells is based on typical semiconductor processing methods (vacuum deposition, CVD, etc.), and hence is relatively expensive to produce. Cells made using organic materials can be fabricated potentially at much lower cost using standard laboratory techniques (spin coating, dip coating, screen printing, etc.) and also offer the advantage of providing a flexible device, of critical importance for select military applications.

One of the leading designs for solar cells based on organic materials is the dye-sensitized solar cell (also known as the Graetzel cell, named after its inventor, Michael Graetzel). This cell is comprised of a porous TiO_2 layer (made using screen printing technologies) with an organic dye molecule adsorbed onto its surface that acts as the sensitizer to absorb sunlight. An electron is transferred from the dye to the TiO_2 and then an electrolyte acts to electrochemically regenerate the dye to complete the circuit. This cell is typically made on a glass support substrate, but recent work has demonstrated that it can easily be fabricated using a plastic substrate for flexible devices. The proposed research will focus on key materials development issues needed to improve efficiencies of these flexible devices into the realm needed for both Air Force and commercial applications. We focused on developing a new class of polymer-gel electrolytes for use in flexible dye-sensitized solar cells in order to boost power efficiencies reaching the 20% level.

2) Technical Approach and Methodology Followed

During the project period several major approaches were followed in parallel to gain more in-depth understanding of the newly evolving field and also to develop solar cells with the maximum efficiency possible. Since the incident photon to current conversion efficiencies (IPCE) of the Ru-dye sensitized solar cells (DSC) already have reached about 90% and cover the entire visible spectral region, the obvious additional gains towards increasing the cell performance are expected only from new hitherto unexplored potential contributing parameters. The major areas thus investigated are:

a) Harvesting the light of longer wavelengths > 700 nm (near-IR). The current Ru-dyes do not harvest these regions. If they are tuned to cover these spectral regions, it will result in lowering the open circuit voltage of the cell.

b) A tandem cell structure, where the Ru-sensitized cell is coupled with an IR light absorbing cell, in principle can deliver higher efficiencies compared to a simple DSC alone. For this to be very highly efficient, the Ru-sensitizers should be able to achieve up to 12.5% conversion efficiency by itself. Therefore, the design of a new class of Ru-sensitizers to achieve 12.5% conversion efficiency was a major component in our research strategy.

c) The second cell of the tandem design could be again a dye sensitized solar cell or an inorganic semiconductor thin film solar cell. Whether the second cell is placed above or below the present DSC, depends on the light absorption characteristics and the I-V characteristics of that cell.

d) A proper current matching between the top and the bottom cells is absolutely essential for achieving maximum conversion efficiencies.

e) For a dye cell to be operative as the second cell, the organic dyes should be capable of absorbing >750nm. Further, they should have a window at the UV-visible spectral wavelengths. These IR absorbing dyes then could be utilized to sensitize a TiO_2 electrode and construct a normal cell as is done so far, for to be used in a tandem device. In this situation the second cell could be placed on top of the Ru- dye sensitized solar cell.

f) An organic dye sensitized solar cell or an inorganic thin film solar cell absorbing near-IR wavelengths transmitted through the top DSC can function as a bottom cell in a tandem structure.

3) Main results

For synthesizing new Ru dyes reaching up to 12.5% conversion efficiency, new ligands have been designed, synthesized and characterized. Using such new ligands new Ru-dyes have been synthesized, characterized and used for making solar cells.

3.1 The need for new dyes:

The standard sensitizers (N719 and Z-907) absorb visible light below 750 nm, which is not sufficient to obtain the maximum possible conversion efficiency from flexible dye-sensitized solar cells. Therefore, it is indispensable to develop panchromatic sensitizers, which harvest solar radiation efficiently in the visible and the near infrared region of the solar spectrum. Design and development of panchromatic sensitizers that absorb visible light of all photons below a threshold wavelength of about 920 nm and convert it into electric current is a goal of high priority. The lowest unoccupied molecular orbitals (LUMO) and the highest occupied molecular orbitals (HOMO) have to be maintained at appropriate levels where both the photo-induced electron transfer into TiO_2 conduction band and the regeneration of the dye by iodide, can take place effectively at 100 % yield. Nevertheless, while maintaining these conditions, it is still possible to further fine-tune the spectral properties of ruthenium polypyridyl complexes in two ways: (1) introducing a ligand with a low-lying π* molecular orbital and (2) by destabilization of the metal t_{2g} orbital through the introduction of a strong donor ligand.

3.2 Ligands required to make ruthenium dyes having enhanced near IR response:

We have used the aforementioned two strategies to modify considerably the MLCT transitions in ruthenium complexes using ligands shown in figure 1. Figure 1 also shows the new dyes synthesized. In the new complexes, 4,4'4''-tricarboxy-2,2':6,2''-terpyridine (**L**) chromophoric ligand tunes slightly the π* orbitals, while the strong sigma-donating spectator ligands (**L1**, **L2** and **L3** in figure 1) destabilize the metal t_{2g} orbitals, resulting indeed in an impressive absorption properties. The extension of the spectral response to the near IR was gained by the upward shifting of Ru t_{2g} (HOMO) levels. However, none of these dyes (N-902, N-907 and 909) performed satisfactorily in solar cells due to various other technical problems.

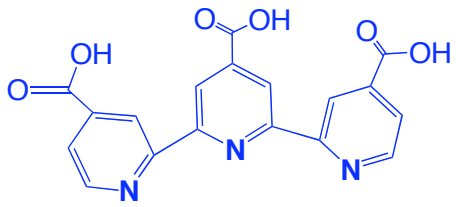

L

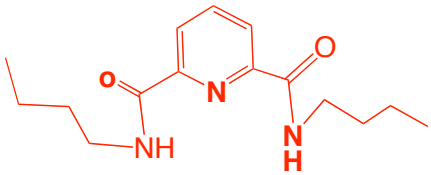

L1

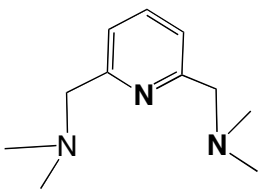

L3

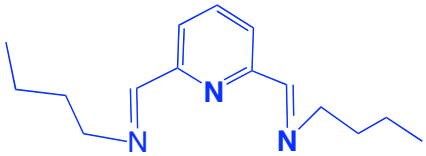

L2

(a) Ligands:

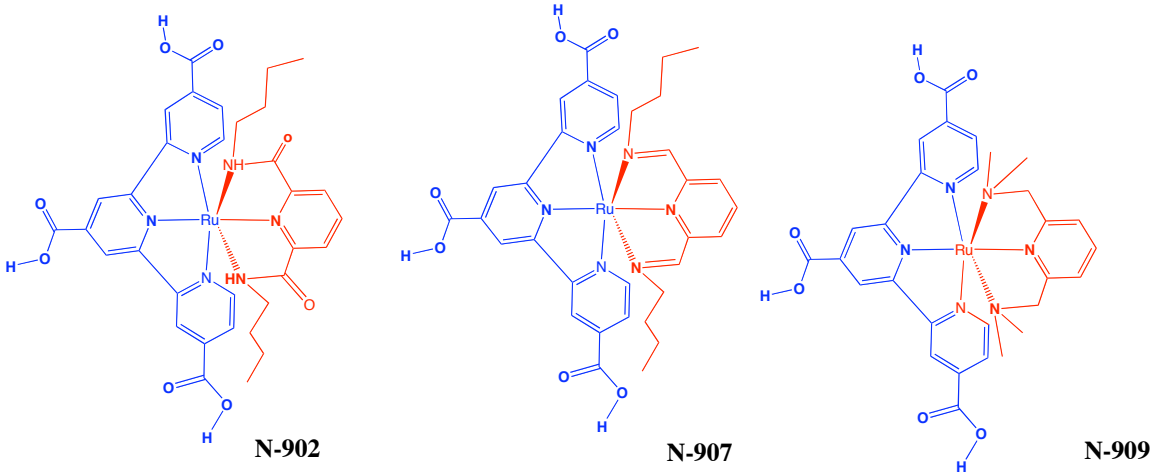

(b) Dyes

Figure 1. New ligands and new dyes for increased spectral coverage

3.3 The Development and Use of Other Panchromatic Ruthenium Sensitizers:

The substituted donor and acceptor groups in tetradentate ligands (figure 2) can also tune metal t_{2g} orbitals and π^* molecular orbitals, respectively, in a "*push-pull*" approach leading to enhanced spectral response in the visible and near IR region. The complexes shown in Figure 2 were therefore used as alternate sensitizers for solar energy conversion. The *trans*-[Ru(L)$(NCS)_2$] complex, shows 75% incident photon-to-current efficiency (IPCE), yielding 18 mA/cm^2 photocurrent density under standard AM 1.5 sunlight. However, the photo-voltage produced by these panchromatic sensitizers reach only 650 mV, resulting in an overall lower efficiency compared to the standard dyes. The most likely reason for such low open circuit potential is the lower LUMO of the quaterpyridyl ligand due to increased conjugation as compared to the standard N3 sensitizer, which has bidentate ligands.

To overcome this problem we have applied two strategies: (a) designing new tetradentate ligands containing oxygen and nitrogen linkers that rupture the conjugation of quaterpyridyl ligands (shown in Figure 3) leading to increased LUMO level, compared to the ligands shown in Figure 2 and (b) the use of co-adsorbents (discussed in section 3.10).

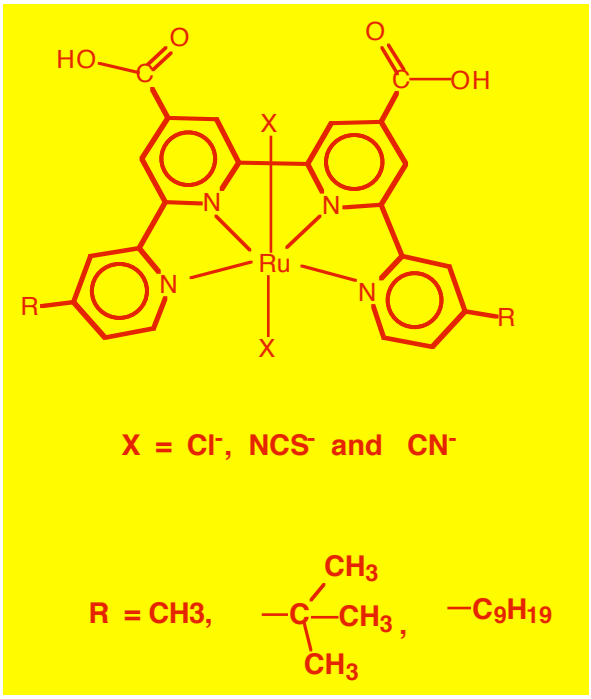

Figure 2. A Ruthenium complex (N-813) containing "push-pull" tetradentate ligands

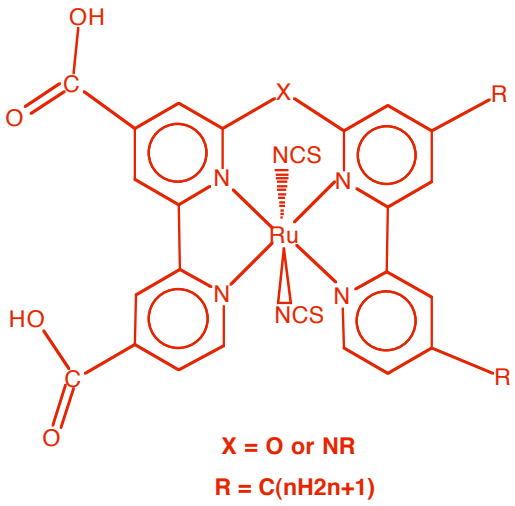

Figure 3. Ruthenium complex with tetradentate ligands containing donor and acceptor groups having oxygen and nitrogen linkers

3.4 Improving the Ru-dye purity:

During this project, we have made significant gains in cell efficiency by other means, which allowed for the first time to reach the 11% mark in standard AM.1.5 (1000W/m2) full sunlight illumination conditions. This progress is achieved by

introducing a surfactant, i.e. the bile acid derivative tetrabutylamonium chenodeoxcholate to the dye solution, and also by improving the purity of the classic N-719 sensitizer. The role of the co-surfactant is to prevent dye aggregation in solution and to facilitate the self-assembly of dye layers on TiO_2 surface.

The proton NMR spectrum of the N-719 dye purified by repeating chromatography on a Sephadex column three times is shown in Figure 4. The inset shows that the region of 7.5 to 10 ppm is practically free from side peaks indicating that the concentration of S-bonded isomer and other impurities is below the detection level. The structure of the chenodeoxycholate additive is presented in section 3.10.

The photovoltaic performance of a DSC using highly purified N-719 sensitizer is shown in Figure 5. For the first time a conversion efficiency of over 11% was obtained in this manner.

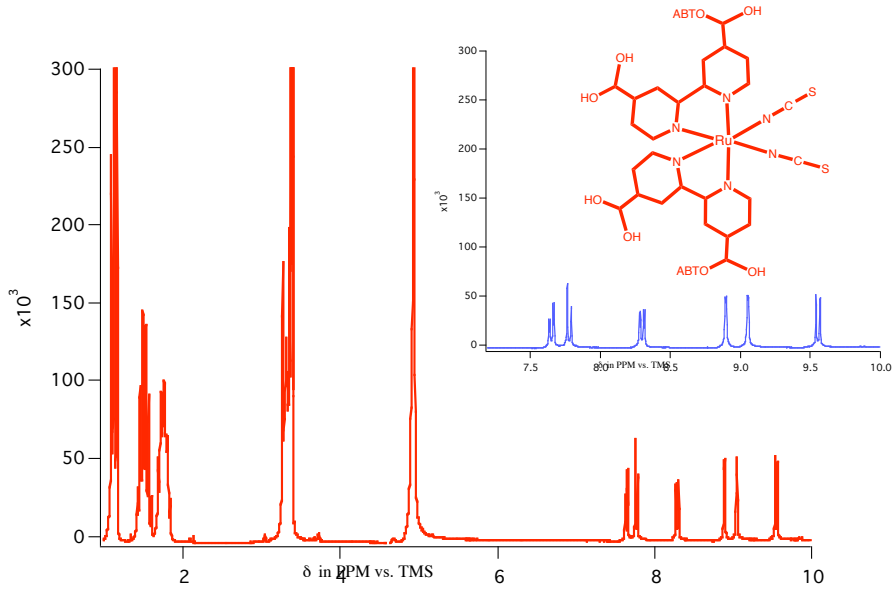

Figure 4. Proton NMR spectrum of the highly purified N-719 dye

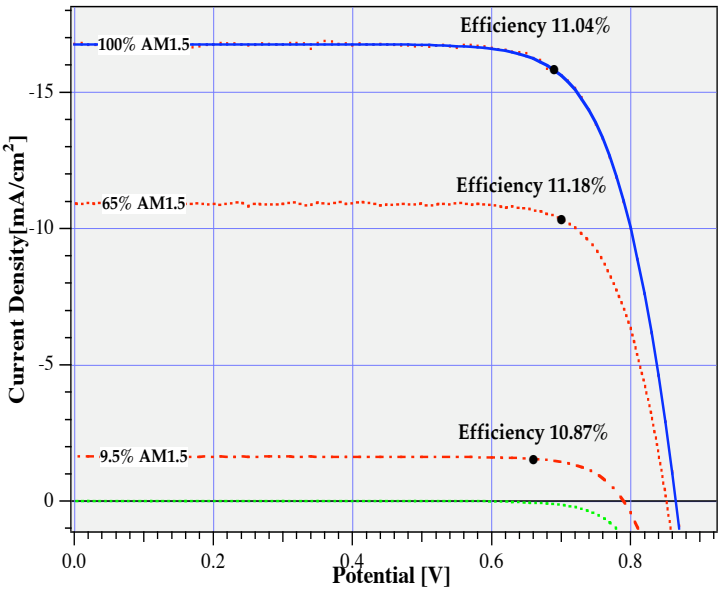

Figure 5: I-V curves of the solar cell which showed 11% conversion efficiency

A systematic investigation of the effect of the purification of dye on the solar cell output was undertaken. Figures 6 and 7 show the effect of repeating the chromatographic purification by a Sephadex L20 column on the short circuit photocurrent and open circuit photovoltage of the DSC, respectively.

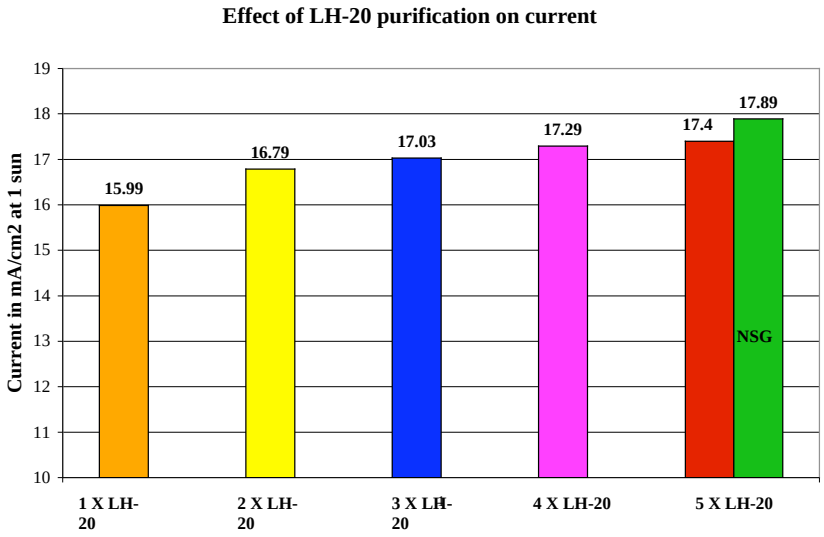

Figure 6. Effect of chromatographic purification of the N-719 ruthenium dye by a Sephadex L20 column on the short circuit photocurrent of the DSC. The green bar on the right side of the diagram refers to a film deposited onto NSG glass

It clearly appears from these results repeating the purification of sensitizer over the L-20 column increases the photocurrent until a plateau is reached after 4 –5- passages. The behavior of the photovoltage is similar except that saturation is attained after 3 repetitions of the purification step.

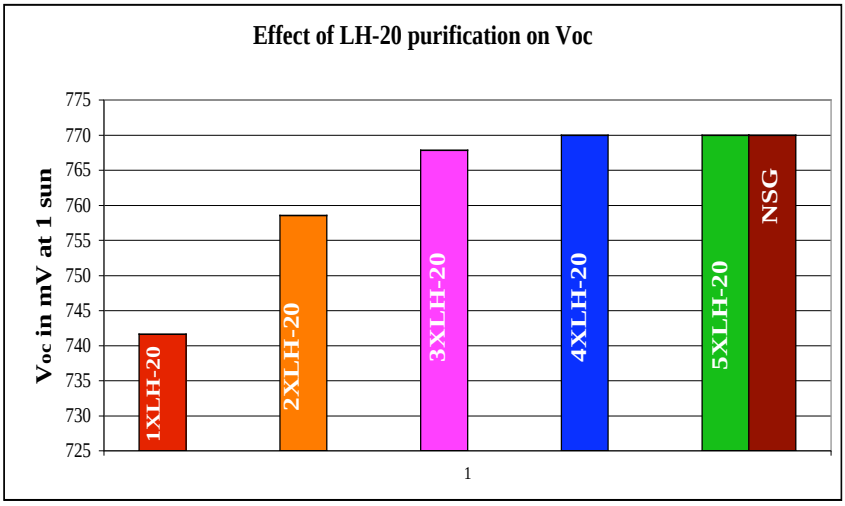

Figure 7. Effect of chromatographic purification of the N-719 ruthenium dye by a Sephadex L20 column on the open circuit photovoltage of the DSC. The brown bar on the right side of the diagram refers to a film deposited onto NSG glass

These results show clearly that the additional purification effort was partly responsible, the other part being the addition of co-surfactant, for the record efficiency shown in figure 5.

3.5 Development of Osmium Panchromatic Sensitizers for Photovoltaic Applications:

In our multipronged strategy of designing and developing novel panchromatic sensitizers that absorb up to 920 nm without significantly altering LUMO and the HOMO levels of metal complexes, some more possibilities exist.

One attractive strategy would be the synthesis of osmium polypyridyl complexes in place of ruthenium. The main advantage of osmium complexes compared to ruthenium is that they are thermally and photo-chemically more stable. The intense main absorption bands, which are present in the ruthenium and the osmium complexes are due to the occurrence of highly allowed singlet electronic transitions. Besides these main bands the Os (II) metal complexes consist of a series of overlapping bands at lower energy in the 600-950-nm region due to direct triplet transitions caused by the heavy atom effect, which are absent in ruthenium complexes. This is another advantage.

Though several osmium polypyridyl complexes are known, only very few have been used as sensitizers in dye sensitized solar cells. Figure 8 shows a representative osmium complex with anchoring ligand developed recently at EPFL. This novel osmium complex with a planar tridentate ligand such as 2,6-bis(1-methylbenzimidazol-2'-yl)pyridine, shows a coordination to the metal in a meridonial fashion. The other three coordination sites in osmium are occupied by bidentate dcbpy and monodentate pseudohalide NCS ligands. Also, the 2,6-bis(1-methylbenzimidazol-2'-yl)pyridine acts as a hybrid ligand having both the strong σ donor (benzimidazole unit) and the π acceptor (pyridine ring) properties. Thus, by an appropriate choice of the substituents on the imidazole nitrogen, it is possible to further tune the ground and

excited state properties in a more predictable manner. The carboxyl groups of the 2,2'-bipyridine ligand provide the grafting functionalities to the oxide surface, ensuring an intimate electronic coupling between the sensitizer and the semiconductor. This type of electronic interaction is required to facilitate the rapid electron transfer between the excited state of the sensitizer and the TiO_2 conduction band. The role of the thiocyanato ligand is to tune the metal t_{2g} orbitals of osmium(II) and possibly to stabilize the hole that is being generated on the metal, after having injected an electron into the TiO_2 conduction band.

The UV-Vis absorption spectra of [OsLL'(NCS)] complex show indeed a series of MLCT bands spanning the whole visible region. Further, an intense near IR band at 856 nm associated to a spin-forbidden triplet MLCT transition is also observed, which is allowed in osmium because of spin-orbit coupling (Figure 9). It is apparent from the spectral data that the osmium complexes play a fundamental role in extending the spectral response in the visible and near IR region due to direct triplet transitions caused by the heavy atom effect (5d metals). Therefore, design and development of this class of compounds and their use in solar cell applications will also be scrutinized in 2004, in addition to the newly planned Ru sensitizers.

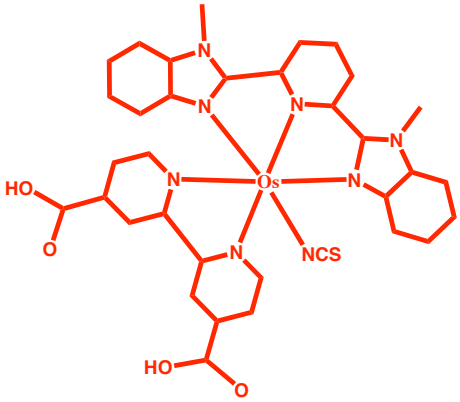

Figure 8. A Representative Osmium complex

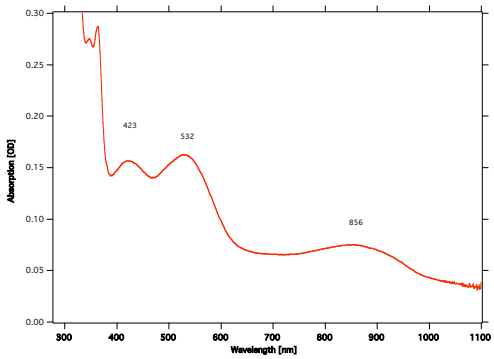

Figure 9. UV-Visible absorption spectrum of [Os(L)(L')(NCS)] complex in C_2H_5OH.

The synthetic work also included carboxylated quaterpyridyl complexes of ruthenium and osmium. Figure 10 shows an example for a new IR sensitizer whose absorption edge successfully extended to 1200 nm by judicious selection of the ligand. This and the related dicyanato complex are presently being tested as charge transfer sensitizers. Electrochemical measurements showed already that a negative shift by ca 0.1 eV of the LUMO-position of the dye will benefit its capacity as a electron transfer sensitizer for TiO2 nanocrystals. Quantum mechanical calculations have shown that the replacement of the tertiary butyl by methoxy groups should produce the desired shift.

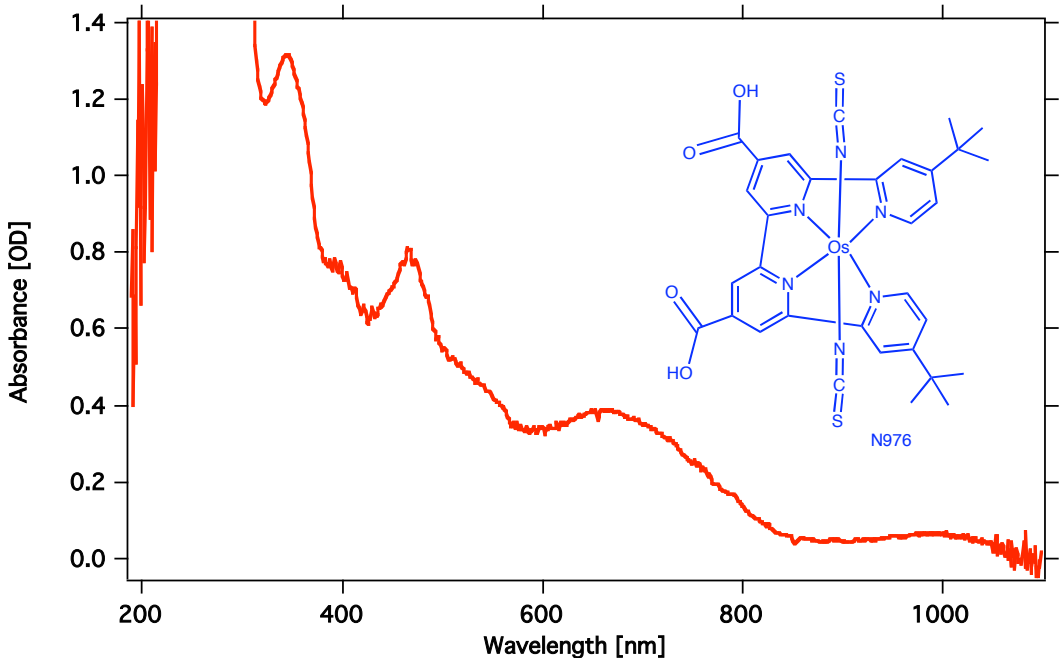

Figure 10. Optical absorption spectrum of a new near IR dye

3.6 New Ru-dyes and better absorption of light:

Having achieved an impressive conversion efficiency of over 11% with the highly purified N719 dye, we have then introduced now alterations in the dye structure to mainly improve its light harvesting in the red region of the visible spectrum and enhance also its relatively low molar extinction coefficient.

The ligands 4,4'-bis(carboxyvinyl)-2,2'-bipyridine and 4,4'-bis(carboxystyryl)-2,2'-bipyridine and their ruthenium complexes **K8** and **K27** were synthesized in two steps as shown in schemes 1 and 2, respectively. The **K8** and **K27** complexes were synthesized in a one pot synthesis starting from the ligand and dichloro(*p*-cymene)ruthenium(II) dimer in DMF for 8h.

Scheme 1

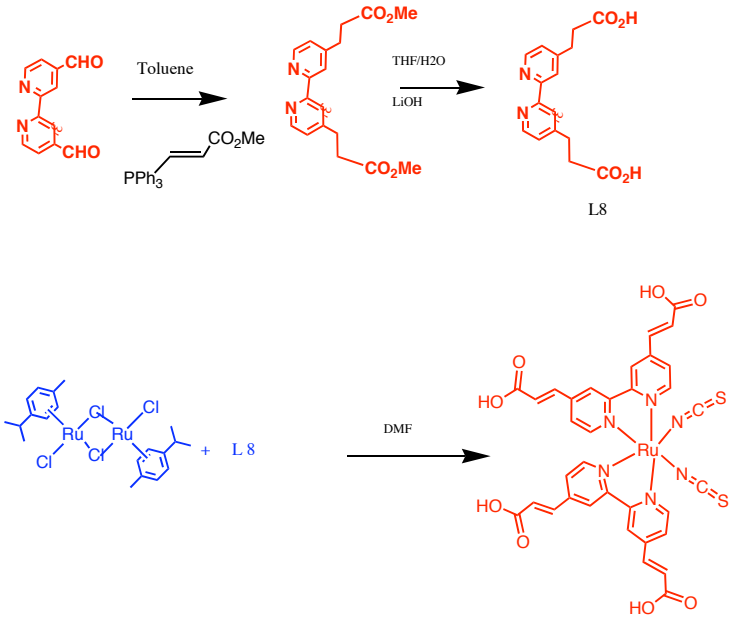

Scheme 2

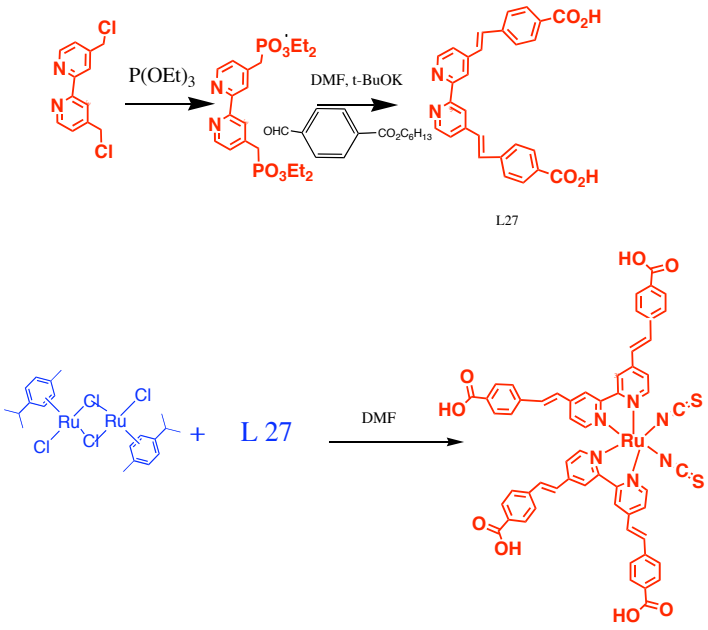

Figure 11 shows structures of the **N719**, **K8** and **K27** complexes. The absorption spectra of the **K8** and **K27** sensitizers are dominated by metal to ligand charge transfer transitions in the visible region at 560 and 439 nm. There are two high-energy bands at 312 and 326 nm due to ligand π–π* charge transfer transitions. A comparison of UV-vis spectra of the **K8**, and the **N719** complexes are shown in Figure 12. The **K8** and **K27** complexes lowest energy MLCT band is red-shifted 30 nm and the molar extinction coefficient increased by 35% when compared to the standard **N719** sensitizer. When the **K8** and **K27** complexes excited within the MLCT absorption

band at 298 K in an air-equilibrated DMF solution, it exhibits a luminescence maximum at 850 nm and a lifetime of 18 (± 1) ns.

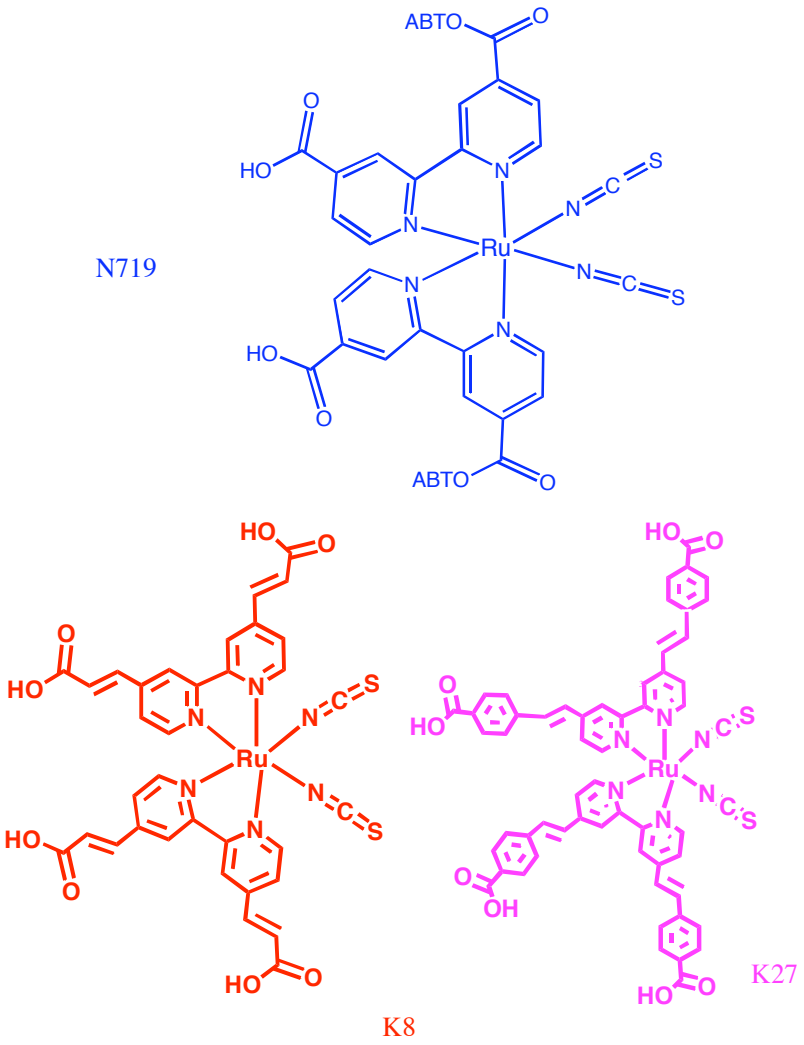

Figure 11. Chemical structure of N719, K8 and K27 complexes

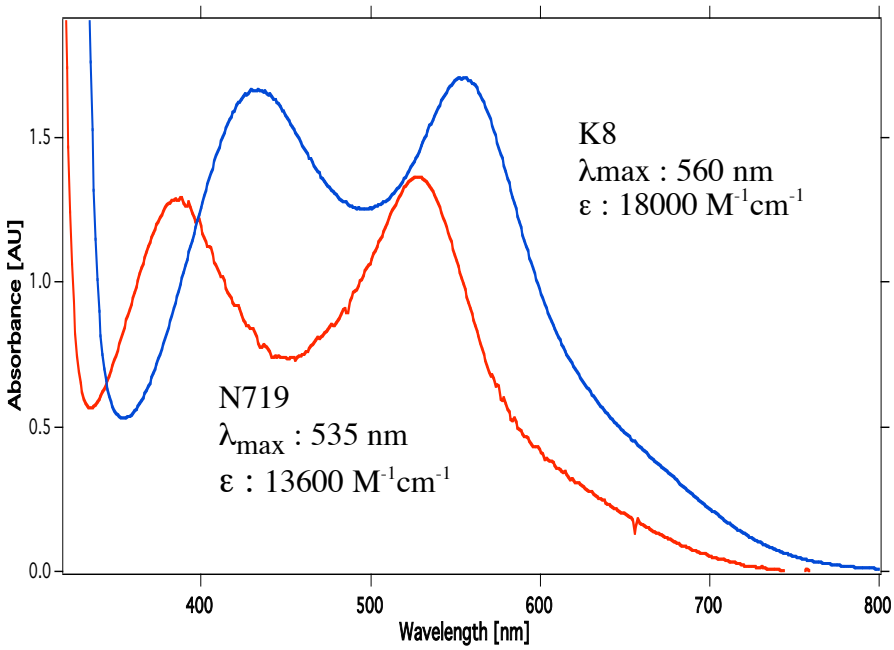

Figure 12. UV/Vis absorption spectrum of K8 complex (blue line, λmax 560 nm, ε 18000 $M^{-1}cm^{-1}$) and N719 (red line λmax 535 nm, ε 13600 $M^{-1}cm^{-1}$) measured in DMF.

The ^{1}H and ^{13}C NMR spectra of **K8** and **K27** complexes measured in dmso-d_6 solution are consistent with the structures shown in Figure 11. The **K8** complex in solution shows 8 peaks in the aromatic region corresponding to the different pyridyl rings and the vinyl protons in which two pyridine rings are trans to the NCS ligands and the remaining two are trans to each other. The proton coupling constant data of the vinyl protons 15.94 and 16.04 Hz confirm that they are in a trans configuration.

The proton-decoupled carbon 13 NMR spectrum of complex **K8** in the aromatic region shows 17 peaks. The carbon-13 data is particularly useful in the **K8** complex for determining whether the NCS ligand has N or S bonded co-ordination. The presence of a peak at 134.4 ppm clearly indicates that the NCS coordination to the ruthenium center is through the nitrogen.

The ATR-FTIR spectra measured in solid sample showed a strong and intense absorption at 2097 cm^{-1} that is due to the N-coordinated υ(CN). This band is approximately 3.5 times more intense than the band at 800 cm^{-1}, due to υ(CS). The band at 1701 cm^{-1} is assigned to the C=O stretching of carboxy groups. The four bands at 1608, 1540, 1472 and 1418 cm^{-1} are due to the ring stretching modes of the ligand. The IR bands at 1635 and 972 cm^{-1} are due to characteristic vinyl (C=C) and trans-(C-H), respectively of 4,4'-bis(carboxyvinyl)-2,2'-bipyridine.

The oxidation and reduction potential data of **K8** and **K27** complexes were obtained using a glassy carbon electrode in DMF solvent with 0.1 M tetrabutyl ammonium perchlorate. Upon scanning to positive potentials a quasi-reversible couple at $E_{1/2}$ = 0.35 V vs. ferrocene (FC) with a separation of 0.09 V between anodic to cathodic peak was observed due to the $Ru^{II/III}$ couple. The ruthenium oxidation potential in complex **K8** is shifted cathodically by 0.05 V, compared to the **N719** complex due to the donor influence of 4,4'-bis(carboxyvinyl)-2,2'-bipyridine when compared to 4,4'-

bis(carboxy)-2,2'-bipyridine. The two reversible waves at $E_{1/2}$ = -1.83 and -2.18 V vs. FC are assigned to the reduction of 4,4'-bis(carboxyvinyl)-2,2'-bipyridine.

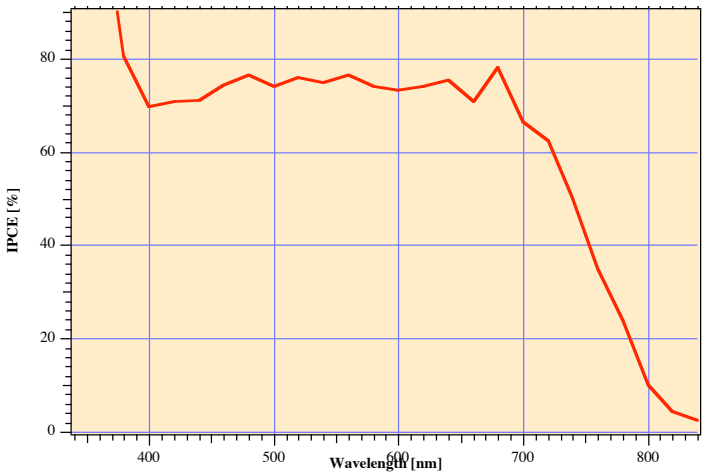

Figure 13. Photocurrent action spectrum obtained with the K8 complex attached to nanocrystalline TiO_2 film. The incident photon to current conversion efficiency is plotted as a function of the wavelength of the exciting light

The solutions of 5 x 10^{-4} M of **K8** and **K27** sensitizers were prepared in 1:1 acetonitrile and *tert*-butanol solution. The photocurrent action spectra obtained with a sandwich cell with based electrolyte (the composition of 1376 electrolyte is 0.6M M-methyl-N-butyl imidiazolium iodide, 0.05 M iodine, 0.05 M LiI and 0.5 M tert.butylpyridine in 50/50 (v/v) mixture of valeronitrile and acetonitrile) under illumination with simulated AM 1.5 solar light. The photocurrent action spectra of **K8** and **K27** sensitizer show broad features covering a large part of the visible spectrum. Figure 13 shows a representative incident monochromatic photon-to-current conversion efficiency (IPCE) plot, which was obtained as a function of excitation wavelength. Strikingly, the incident monochromatic photon-to-current conversion efficiency show in the plateau region close to and even at 700 nm the value is 66%. From the overlap integral of this curve with the standard AM 1.5 solar emission, one derives a short circuit photocucrrent densitiy of 18.1 mA/cm^2. In agreement with this measurement under the standard global AM 1.5 solar conditions, the cell gave a photo-current density of 18±0.5 mA/cm^2, which is significantly higher than the N-719 analogue. The enhancement asserted by the ligand containing an extended conjugation is evident from the IPCE spectrum in the red region.

3.7 A new porphyrine sensitizer with enhanced near IR response:

In collaboration with Prof. David Officer from Massey University New Zeeland, a porphyrine dye of intense green coloration was discovered for DSC applications, whose structure is shown below. The substitution of one of the pyrrole moieties of the porphyrine by a cyano-acrylate acid group leads to a red shift in the position of the Q-band.

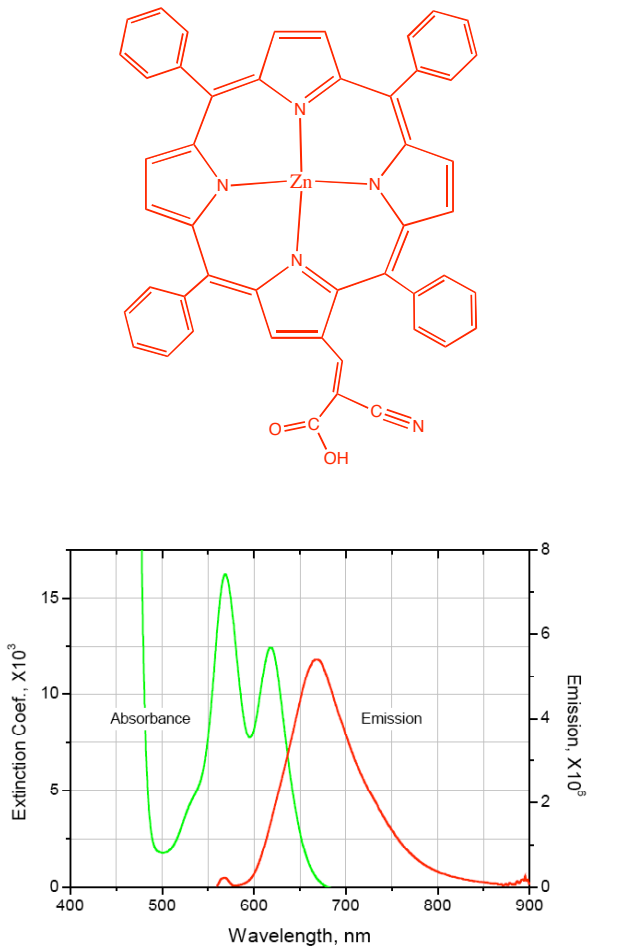

Figure 14. Molecular structure and the absorption and emission spectra of the new porphyrine dye showing enhanced near IR response

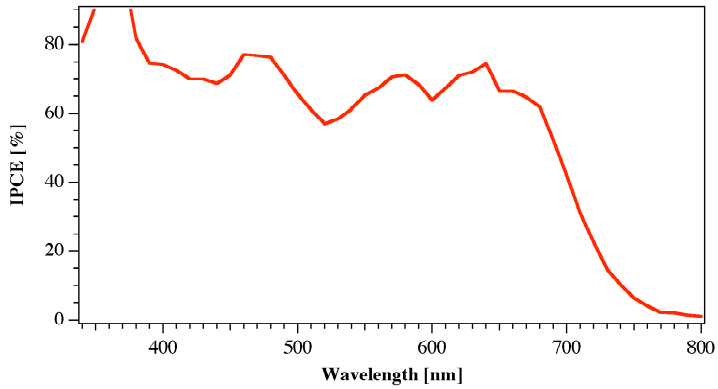

Figure 15. Photocurrent action spectrum of the new porphyrine dye showing incident photon to current conversion efficiencies (IPCE) close to 80 percent

At the same time, the intensity of the transition is enhanced. Figure 14 shows the molecular structure and, the absorption and emission spectra of the new sensitizer, while Figure 15 presents the spectral response of the photocurrent. Very high external quantum efficiencies approaching 80% were obtained. This new green phorphyrine shows great promise as a co-sensitizer for increasing the solar light harvesting of the dye sensitized solar cell.

One of the most useful dyes, other N3 for DSC applications is the K-19 dye. The structure of the K-19 dye is shown below:

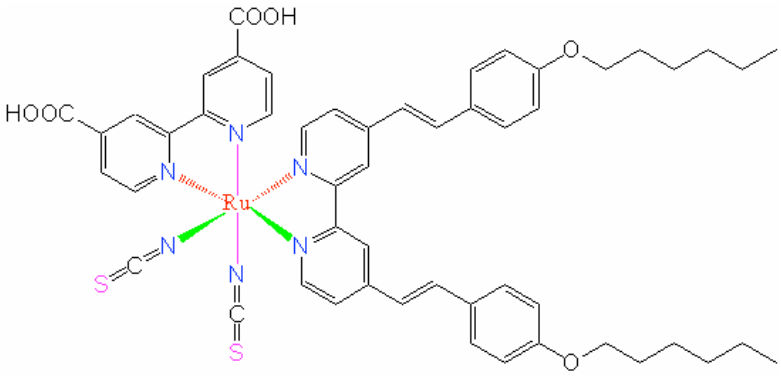

Synthetic efforts have aimed at improving further the previously employed K-19 dye. Replacement of the benzene of the latter by naphthalene leads to the new sensitizer coded K-24.

K-19

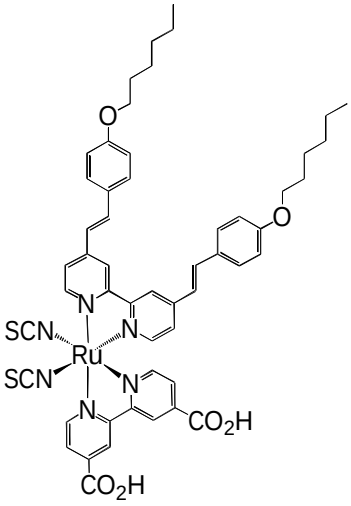

K-24

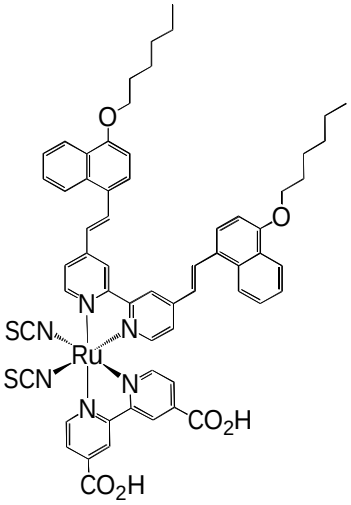

The main advantage of the K-24 with respect to the K-19 dye is the increased light harvesting in the 380 to 450 nm region, which is beneficial to the photocurrent as it compensates the significant filter effect of the triidodide/iodide redox electrolyte in this spectral domain. This can be seen from a comparison of the absorption spectra of the two dyes shown in Figure 16. First photovoltaic results with the K-24 sensitizer appear promising.

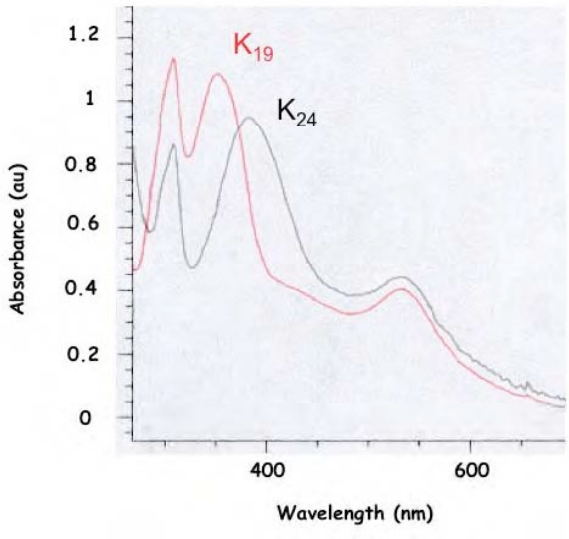

Figure 16. Comparison of the absorptions spectra of the K-19 and K-24 dyes

3.8 Dye cocktails:

To improve the longer wavelength light harvesting capacity of a DSC in the 650 - 750 nm range, a dye cocktail has been applied and studied.

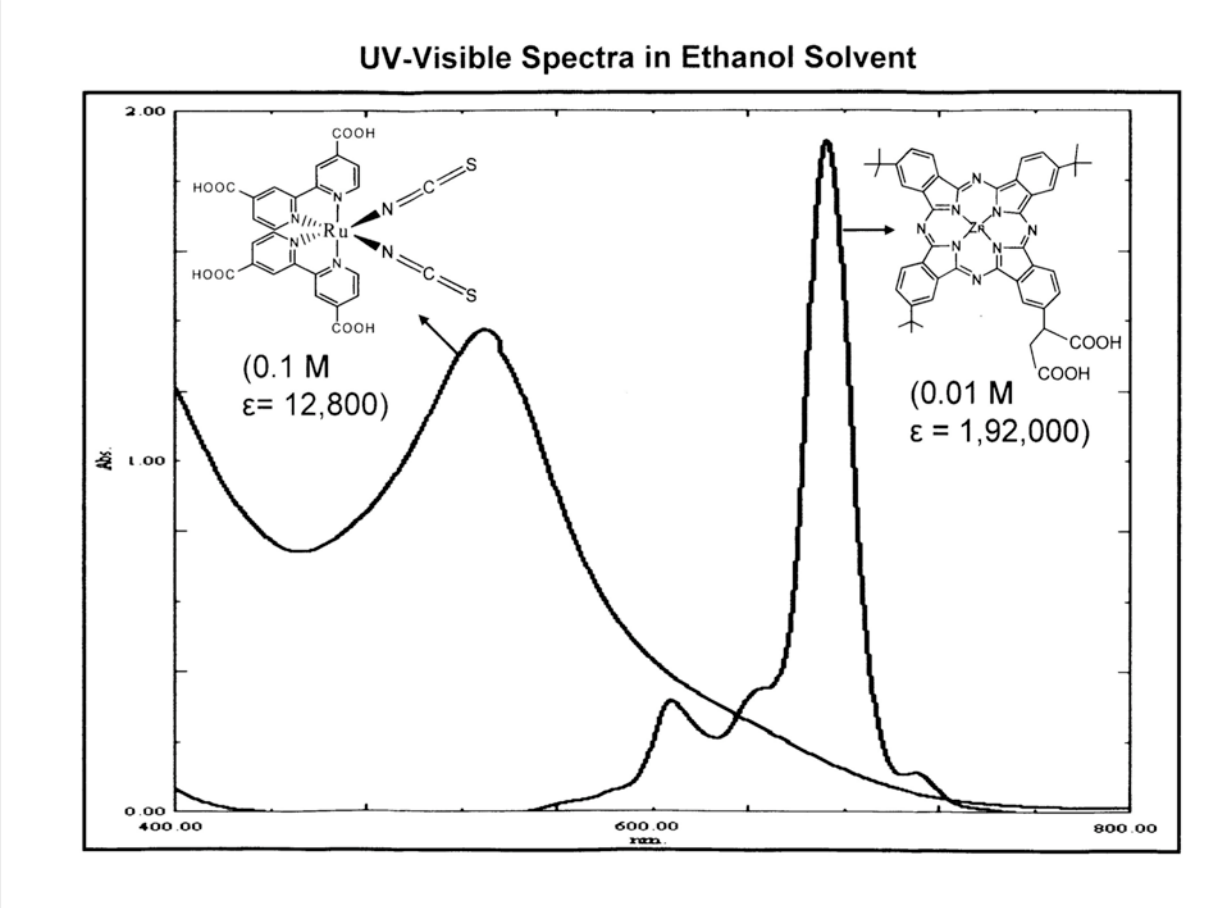

Figure 17. Absorption spectrum of a new phthalocyanine sensitizer along with that of a ruthenium complex

It is clear from the comparison of the two spectra shown in Figure 17 that the phthalocyanine (PC) provides a strong absorption feature in a spectral range where the light harvesting by the ruthenium complex is weak. Since the maximum extinction coefficient of the PC is more than 10 times higher than that of the ruthenium dye it should suffice to cover only 5 -10 % of the TiO_2 surface with the co-sensitizer to achieve efficient light harvesting.

These expectations were borne out by the results from phototvoltaic measurements using a dye cocktail of the two sensitizers to color the transparent titania electrode Results are shown in Figure 18, where the incident photon to current conversion efficiency (IPCE) is plotted as a function of wavelength. The appearance of a spectral maximum at 680 nm clearly shows that the co-sensitization by the phthalocynanine is operative producing enhanced response of the photocurrent in the red region of the spectrum.

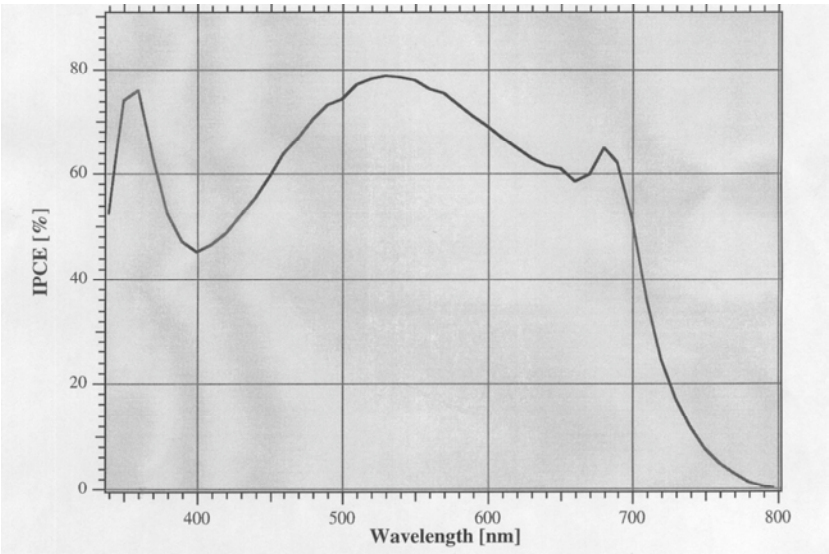

Figure 18. IPCE spectrum of the DSC cosensitized by the ruthenium dye Z719 and the phthalocyanine. The latter contributes the 680 nm feature to the photocurrent.

3.9 Organic Dyes for selective IR light absorption:

High efficiency and thinner layers of TiO_2 in solar cells are both required for using an organic dye sensitized mesoscopic solar cell as one of the cells in a tandem device. For this purpose, dyes with high extinction coefficients are required. The squaraines, being organic dyes, have very high extinction coefficients in the region of > $200000 cm^{-1} mol^{-1} dm^3$ allowing the use of much thinner TiO_2 layers in the cells, whilst retaining the high OD required for effective photon to current conversion efficiency. The dyes are also more easily tuneable toward the near infrared than the standard ruthenium dyes, thereby increasing their light harvesting potential. The new organic dyes will have absorption maxima between 680-850nm with spectral broadening and J-aggregate shifts expected to accompany the adsorption of the merocyanine analogue

dyes on the surface of TiO_2. Taking this into consideration these dyes were expected to have a reasonable IPCE value at or above 900nm. The dyes may also help pave the way toward transparent IR solar cells. We researched elaborately on squaraine dyes during this project period.

The general structure of the organic dyes studied is shown below:

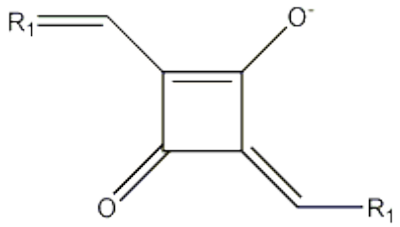

The work involves the synthesis of several indolene and benzazole analogues (R_1) of the squaraine dyes and work is presently carried out to optimise the attaching groups and functionalities localised on R1 to improve injection and again the overall light harvesting efficiency.
The first dye produced (B1) is a derivative of benzindolene. A photo of the dye dipping solution (Figure 19) and the abs max in methanol (Figure 20) are shown below. The product has been characterised with H^1 NMR, UV-VIS spectroscopy, elemental analysis, mass spectroscopy, C^{13} NMR and cyclic voltammetry.

Figure 19. Squaraine dye solution ($2.5x10^{-4}M$) in THF:EtOH

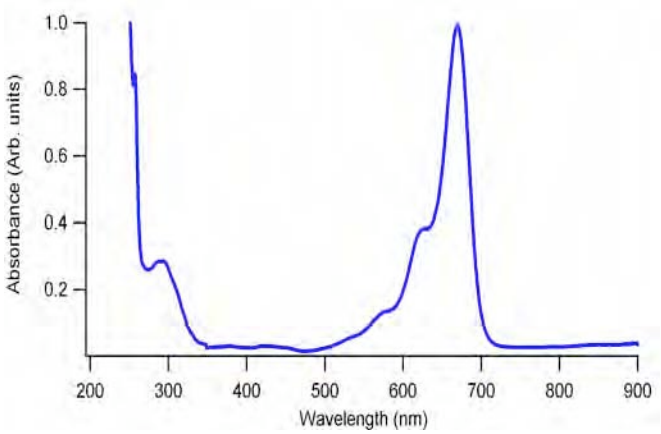

Figure 20. Abs spectrum of B1 in Methanol.(7:1) and chenodeoxycholic acid as the co-adsorbant

The original idea was to use these dyes along with Ru dyes or in cells placed tandem to Ru dye cells. Before proceeding to that stage, this new dye has been tested for its individual performance in solar cells. We measured efficiencies just over 3%. Typical I-V curve and IPCE data are shown in figures 21 and 22. The 3% efficiency will be enough to augment the overall performance of a Ru dye based solar cell, when it is arranged in tandem mode. However, for this final goal, it would be better to shift the absorption spectrum of the dye further more to longer wavelengths. This will have to be achieved with suitable structural modifications.

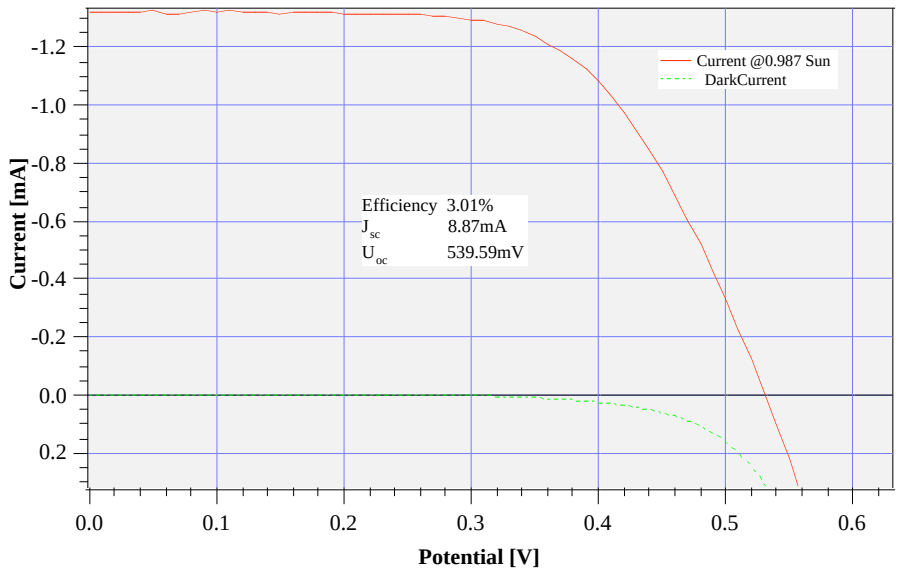

Figure 21: IV curve of the B1 dye adsorbed on a 8μ TiO_2 photoelectrode containing a 4μ scattering layer and compact blocking layer on the conducting glass surface. The electrolyte used was similar to the standard electrolyte used for Ruthenium sensitised cells though no t-butyl pyridine was present. The cells were dipped for 1hr in the same $2.5x10^{-4}$M THF:EtOH solution

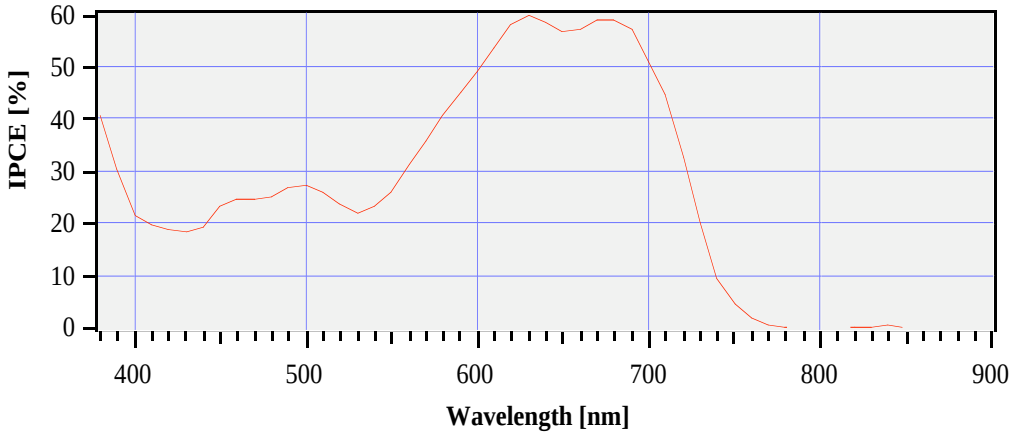

Figure 22: IPCE of the same cell used above in figure 21

It was expected that further purification of the dye, an optimisation of dipping times, TiO_2 layer thickness and optimisation of the concentration of co-adsorbant used to prevent aggregation should lead to considerably higher efficiencies. The higher extinction co-efficient of the B1 dye with respect to the standard ruthenium dyes should increase the optical density of the films and hence the IPCE and efficiencies of the cells.

Further, more new dyes were produced using the same basic structure but with required modifications including the introduction of thiophenes to broaden the spectral absorption characteristics and alternative chain lengths and positions for the carboxylic acid anchoring groups to increase the rate of electron injection.

The first dye produced was a derivative of benzindolene. A variation of the first dye was prepared by reacting N-propyl-3-carboxy-2,3,3-trimethyl-5-thiophenylindole with squaric acid to yield another desired squaraine shown below.

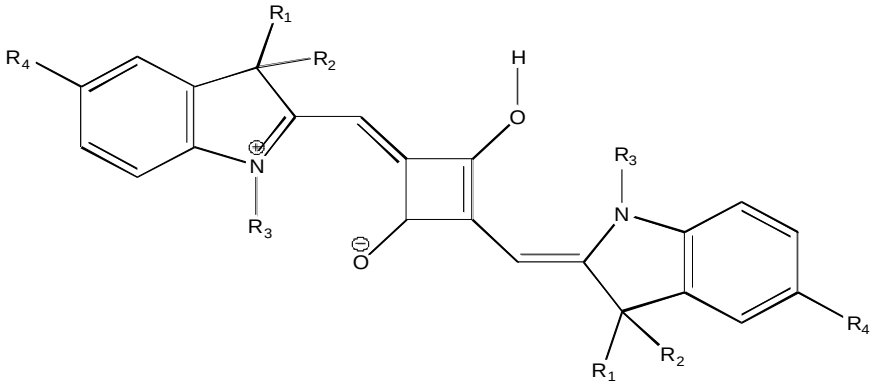

In this series of the squarine dyes, R_1 and R_2 are generally alkyl groups, R_3 is a nonconjugated alkyl chain with the respective attachment group and R_4 can be alkyl, phenyl, thiophenyl etc. In the case of the reaction above R_4 is a thiophene moiety.

Again the product is a brilliant blue due to its narrow absorption peak with λ_{max} 664 nm (Figure 23), which is only 6 nm blue shifted in comparison with the benzindole

product shown earlier. The next step is therefore the addition of a further thiophene or thiophene carboxy ring, which should shift the absorption a further 35 - 40nm towards the red.

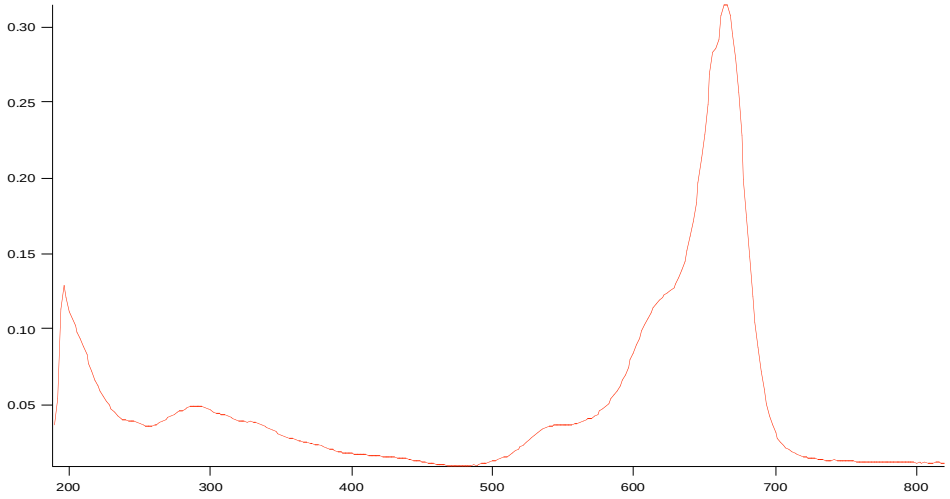

Figure 23: Dye bis(N-propyl-3-carboxylicacid-2,3,3-trimethyl-5-thiophenylindole) squaric acid was initially purified via precipitation under acidic conditions. As has been seen for the propyl and ethyl analogues the product is a brilliant blue in ethanol.

The reaction to form the simple squaraine, bis-(2,3,3-trimethyl-5-pyrenyl-3*H*-indole) squaraine was tried The product B9 had approximately the same $\lambda_{\mu\alpha\xi}$ as the dyes B1 and B2 reported earlier as shown in Figure 24 below. This suggests that an alternative method should be found to shift the absorption further toward the IR.

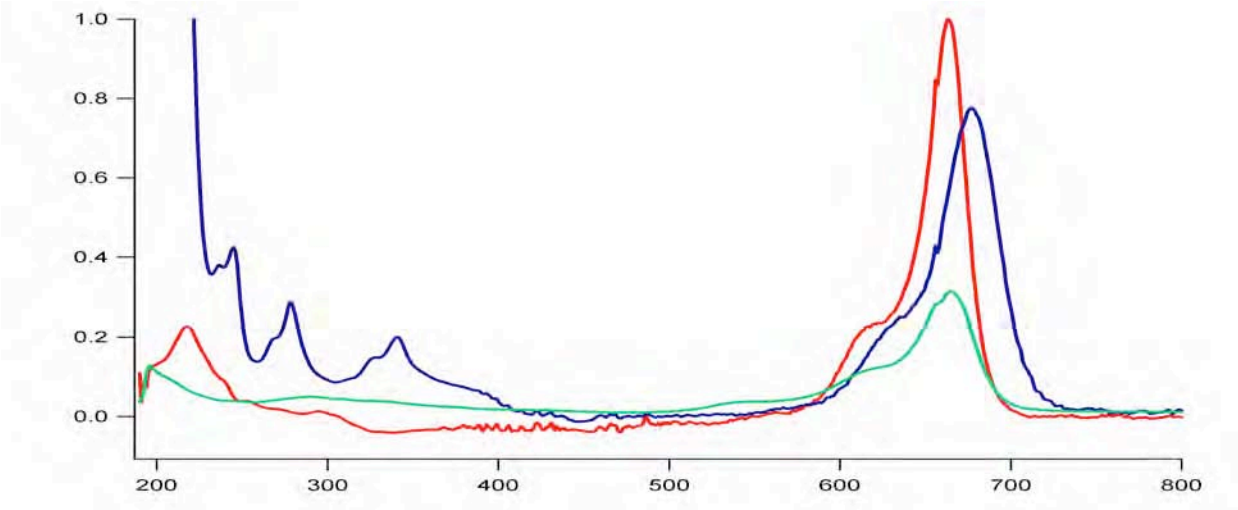

Figure 24. UV-VIS spectra of B9 bis-(2,3,3-trimethyl-5-pyrenyl-3H-indole in dichloromethane (blue line) as can be seen the abs max is at approximately the same wavethength as for the dyes B1 and B5 (EtOH). The apparent red shift is due to the fact that DCM was used in place of EtOH for B9 as it was not soluble in EtOH.

MO calculations with Cache had shown that a small proportion of the electron density resided on the benzene moiety on the benzindole and on the thiophene in the case of

the thiophene indole products. Subsequent calculations using the pyrene squaraine however confirmed these results showing effectively no conjugation with the squaraine unit in the lowest energy HOMO-LUMO transition. Work has therefore concentrated on extension of the methine chain sections of the dyes. A literature search has shown a few dyes, which could effectively be used in solar cells. These dyes lack the suitable carboxylic acid attaching groups and which therefore requires to be added.

After a series of painstaking synthetic work, a final dye has been produced through the reaction of the synthesized 2-methyl-α-napthothiazolium iodide and N-(2,5-dianilinomethylenecyclopentylidene)-diphenylaminium perchlorate in ethanol. The dye has an absorption max at 830nm with a tail to ~900nm in MeOH (see figure 25). On the surface of TiO_2 this should be extended further to ~940-960nm. The purification of this particular dye was relatively simple due to its exceptionally low solubility especially with respect to the imputities. The dye coded B10 was isolated as a golden powder that formed a blue green solution in MeOH.

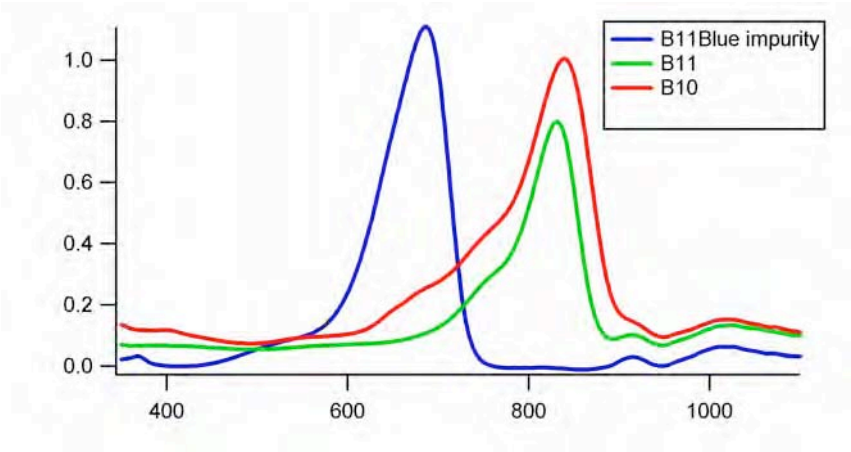

Figure 25. UV-Vis of the products B10 and B11 note the absorbance is arbitary and has not been normalized ie the concentrations of the species vary. Note also that the slight shift in the peaks for B10 and B11 are solvent related. The X-axis is wavelength in nm and the Y-axis is arbitrary units showing the intensity of absorption.

This dye is very soluble in many of the standard solvents i.e., DCM, MeOH etc. Though due to its high solubility it has proved difficult to isolate and requires some 6 individual steps to do so. It can be seen from the NMR that the product is nearly pure.

The work related to dyes absorbing light in the red and near-IR regions continued. As it was shown that the dyes with an extended conjugation on the indole moiety showed no significant red shift of the absorption maxima, new dyes were produced with the general formula:

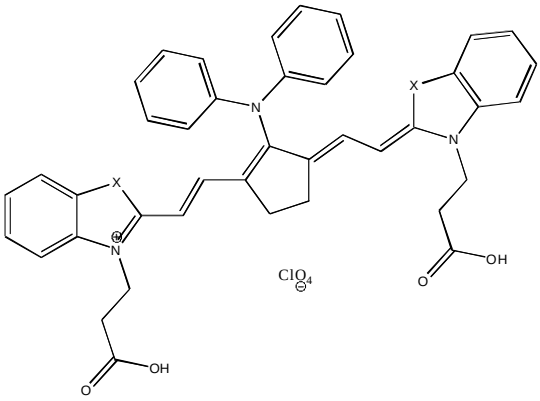

Figure 26 – General structure of the dyes B10-B11. Here X=C(CH$_3$)$_2$, S

Here benzoindole and indole analogues of the dyes have been made. B10 involved a benzothiazole and the dye B11 a 1,2,2-trimethylbenzo[e]indole functionality. The dye B12 involved a thiazole ring.

The final dyes with the exception of B12 proved difficult to purify. The dye B12 did not suffer as badly as B10 and 11 respectively and could be purified with relative ease. The UV Vis spectra of the dyes B10-12 are shown below. The blue shift of the dye B12 relative to the others is due to extended conjugation through the benzene ring present in the latter two dyes.

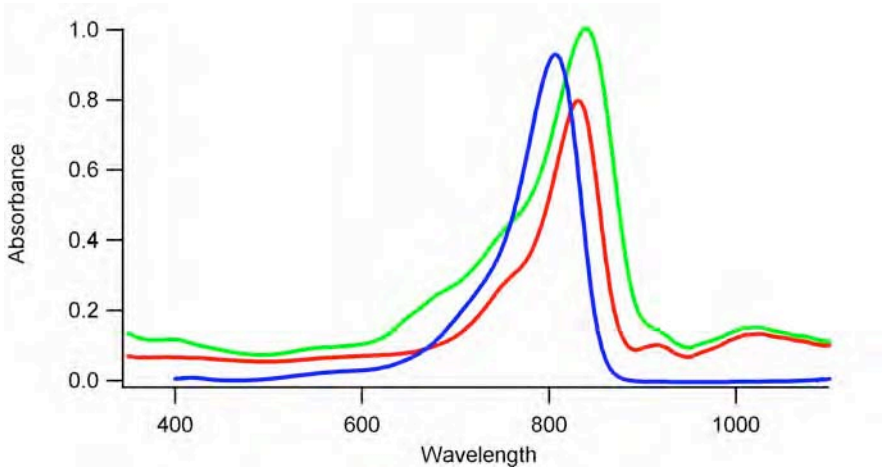

Figure 27– Absorption spectra of the three dyes B10 (Green), B11 (Red) and B12 (Blue). Spectra have not been normalized.

The dyes B10-12 were tested electrochemically. Since the solubility varied greatly between the dyes, the availability of solvents to be used in CV measurements is limited. The CV for B10 could not be measured, as the product was only soluble in H_2O. Figures 28 and 29 show the CV data for B11 and B12.

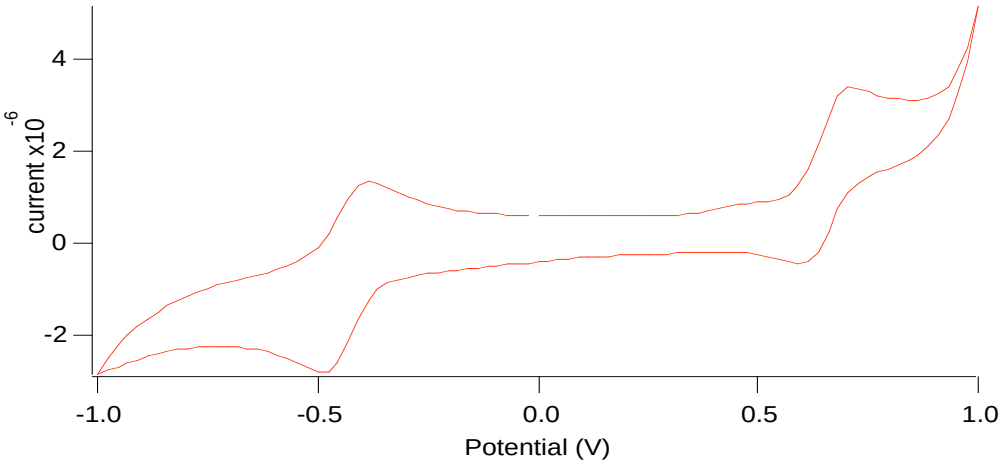

Figure 28 –CV of the dye B11. The reference used was ferrocene. The actual peak of the ferrocene was at the same potential as the oxidized state of the dye and was hence not shown. Note that the CV was measured in DMF.

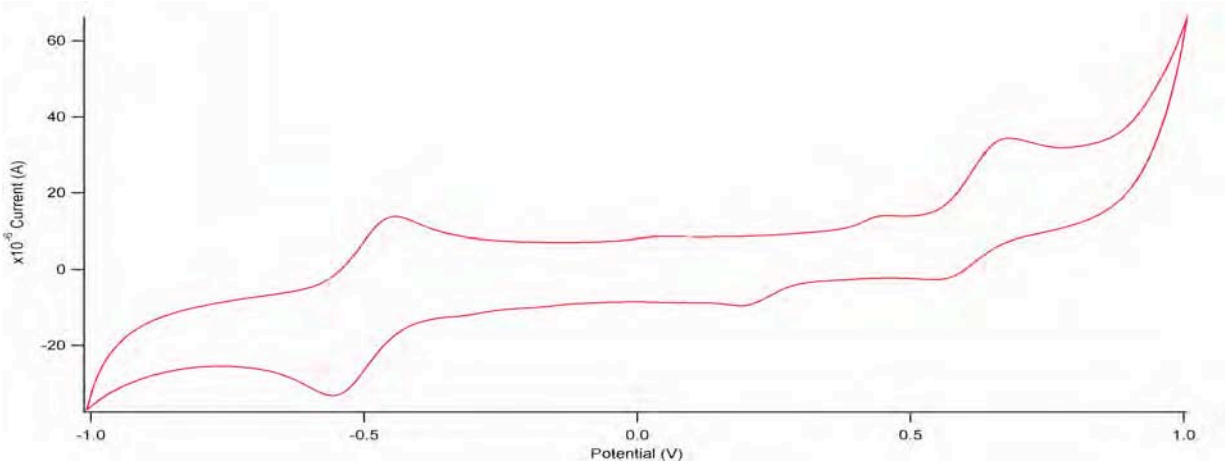

Figure 29 – CV of the dye B12. The reference used was ferrocene. The actual peak of the ferrocene was at the same potential as the oxidized state of the dye and was hence not shown. Note the CV was done in MeOH.

The HOMO level is calculated as +0.46V vs SCE, and the LUMO, of the reduced state, lies at -0.99V. Unfortunately neither B11 nor B12 worked with the iodine/triiodide couple.

Another new dye has been synthesised, incorporating a diethyl carboxy functionality on a squaraine central unit, to absorb wavelengths >700nm. It is thought that the

LUMO is found in the centre of the methane chain. This would decrease the distance for charge injection to the TiO_2 photoelectrode. The substitution of the O- for a NR2 group also shifts the absorption of the respective compound 20-30nm further toward the red. The general structure of the dyes is shown below:

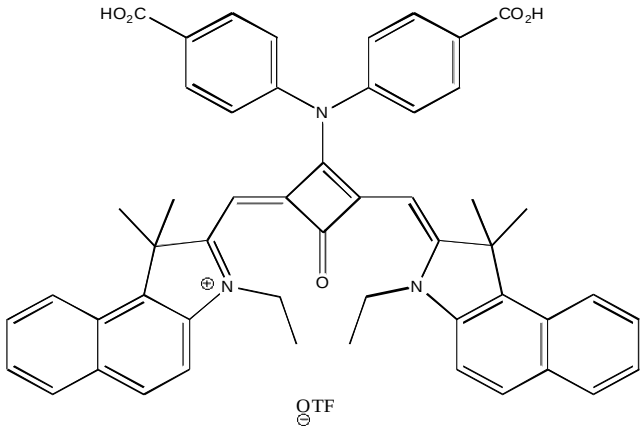

Figure 30. General structure of amniosquarilium dyes

The synthesis of several dyes was attempted with the initial synthesis involved the formation of the N-ethyl indolium salt:

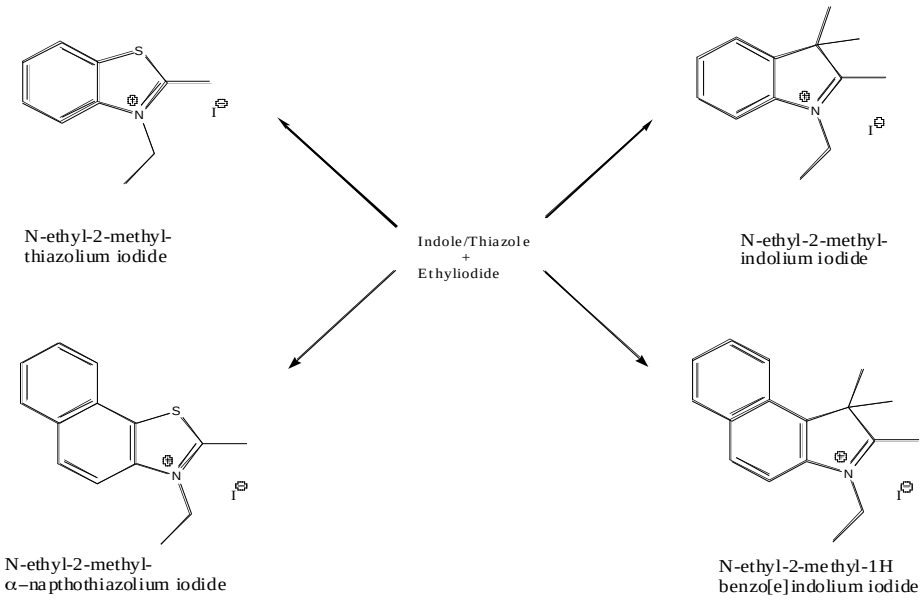

Figure 31. General structures of starting materials

The intermediates above were all characterized via H^1 NMR, CHN and Mass spec. The product N-ethylthiazolium iodide was obtained pure. The next stage in the synthesis involved the formation of the squaraine. Here 2 equivalents of the indolium salt and squaric acid were heated together under reflux with the azeotropic removal of water from the reaction mixture.

The products bis(N-ethyl-2,3,3-trimethylindole) squaraine and bis(N-ethyl-2,3,3-trimethy-1H-benz[e]lindole) squaraine were easily isolated and purified. The two products involving the thiazole and napthothiozole squaraine products could not easily be isolated and proved considerably less soluble. These were not worked up further.

The next step involved the synthesis of the O methylated product of the squaraine to give the corresponding methylated squarilium dye. The synthesis involved the reaction of the squaraine with methyl triflate. Only the product from the reaction of bis(N-ethyl-2,3,3-trimethy-1H-benz[e]lindole) squaraine was formed. However, this was easily purified and the spectrum of the product is shown below.

The final step in the synthesis of the dyes is the addition of the attaching group; in this case, the reaction with 2,2-iminodibenzoic acid was tried. The reaction, however, did not work and was stopped after 3 days. This was possibly due to the fact that the lone pair on the nitrogen was not free due to the conjugation with the benzene rings. The next reaction that was tried involved 4-aminocinnamic acid this was tried as both the amine and in the form of the HCl salt as this was thought to catalyse the condensation reaction. Neither of the reactions however worked. It was then decided to simply react the methylated squaraine with diethyl iminodiacetate. This would not shift the absorption as far as the diphenyl analogue but still shifts the product 20-30nm toward the red. The two carboxy chains are also situated on the squaraine centre. The product unlike B1 was very easy to produce and purify and required only one pass through a reverse phase column. A small sample of the nearly pure dye directly from the column was tried in solar cells. The dye gave over 60% incident photon to current conversion efficiency in the initial tests in the wavelength range over 700 nm and looks very promising after further structural modifications.

In effect, in DSC applications none of these new organic dyes performed as desired. They also suffered from other problems such as stability, difficulty in purification and poor binding with TiO_2. More work is needed to develop the most appropriate organic dye, which can efficiently harvest the radiations beyond 700 into the IR region.

So far our screening has identified the purified N3 and the K19 as the best dyes. Both dyes contain ruthenium.

3.10 Use of Co-adsorbents:

The aim of using co-adsorbent with the dye is to suppress the pinholes left on the surface of the TiO_2 after the dye sensitization. These pinholes are the source for the increasing dark current due to the back electron transfer from TiO_2 conduction band to the electrolyte. It is imperative to stop this back electron transfer to enhance the photovoltaic performance of the cell. Among the coadsorbents investigated, guanidinium butyrate has given the highest open circuit voltage so far, reaching values of up to 0.86 V. The measurements also showed clearly a decrease in the dark-current, where the onset potential for the reduction of triiodide shifts negatively. In this manner, we have made significant gains in cell efficiency, which has passed for the first time the 11 percent mark in standard AM.1.5 ($1000W/m^2$) full sunlight. This

progress was achieved by introducing a surfactant, i.e. the bile acid derivative tetrabutylamonium chenodeoxcholate to the dye solution and by improving the purity of the N-719 sensitizer. The role of the co-surfactant is also to prevent dye aggregation in solution and to facilitate the self-assembly of dye layers on TiO_2 surface. The chemical structures of the two most useful co-adsorbents are shown in figure 32.

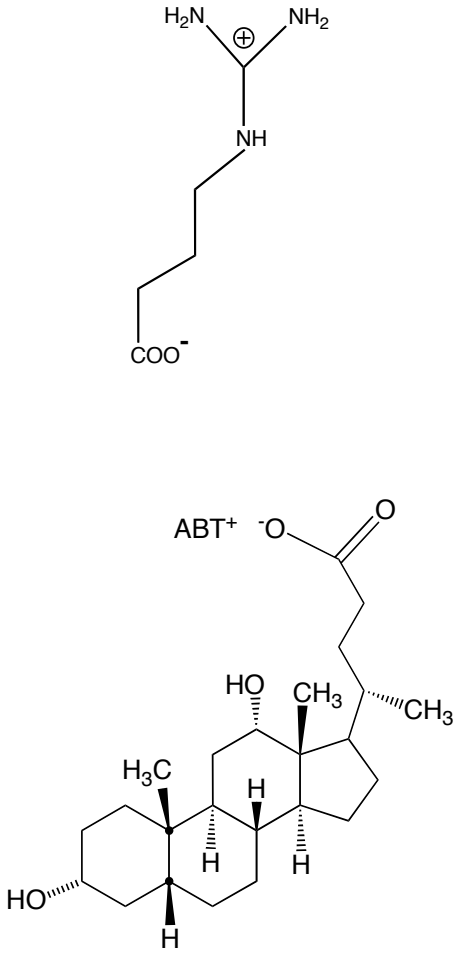

Figure 32. Structures of 4-guanidinobutyric acid (GBA) (top) and chenodeoxycholate (bottom) used as co-adsorbents in dye sensitized solar cells

3.11 Beneficial changes during the aging of freshly prepared cells:

The mechanism of initial aging of freshly prepared cells has been investigated, in order to understand the changes occurring on the various interfaces (electrode-electrolyte and dye-TiO_2, for example). Some relevant experimental data are shown in Figures 33 and 34. Remarkably, all photovoltaic cell parameters, i.e. the short circuit photocurrent (Isc), the open circuit photo-voltage (Voc) and the fill factor (ff) show an improvement during the first 60 hours of aging resulting in an efficiency increase from 9.6 to 10.8 percent. This initial gain in efficiency can be ascribed to a lateral spreading of the dye on the nanocrystalline titania surface. Laser photolysis studies point to the initial presence of dye aggregates at the surface of the

nanocrystalline TiO_2 films. As the cell matures the dye spreads at the interface forming a monolayer. The self-assembly of the molecular dye layer is assisted by the guanidinium ions that are added to the electrolyte. The presence of a dye monolayer impairs the access of triiodide ions to the surface reducing the dark current at the interface. This is shown by the green curves in Figure 34. As a result there is a net gain in the open circuit voltage and power output of the cell.

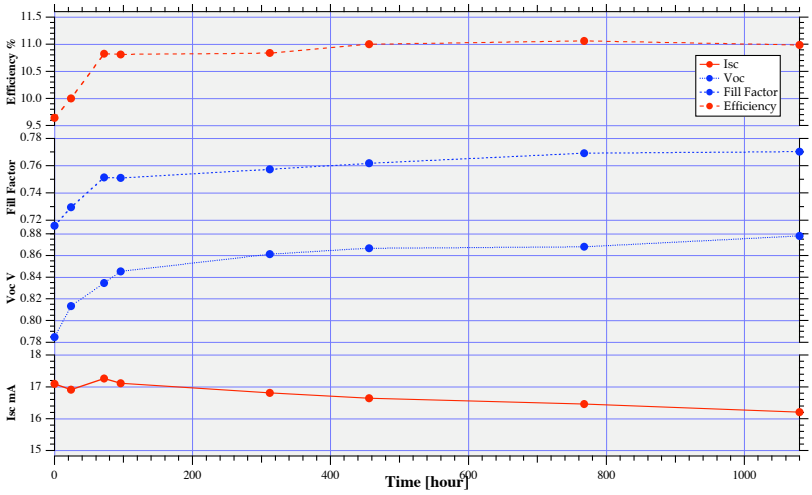

Figure 33. Effect of aging at room temperature on the photovoltaic performance of solar cells. The electrolyte contained 0.5 M guanidinium thiocyanate which assists self assembly of the sensitizer. The sensitizer was N719 purified 3 times over a Sephadex L20 column

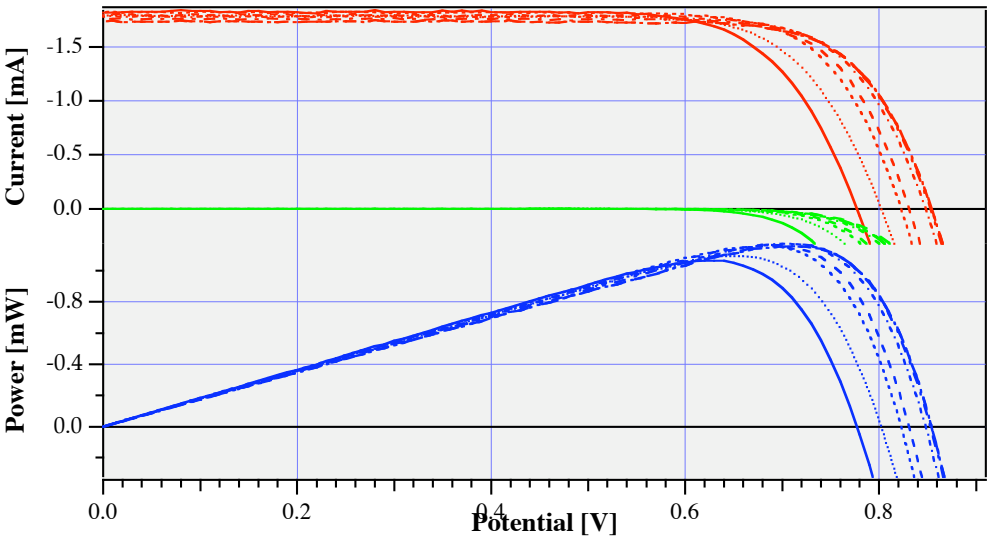

Figure 34. Effect of aging at room temperature on the indicidual photovoltaic performance of solar cells. The electrolyte contained 0.5 M guanidinium thiocyanate, which assists self assembly of the sensitizer. The sensitizer was N719 purified 3 times over a Sephadex L20 column. The green curves in the upper diagram present the dark current. The device size was 0.162 cm^2.

During the second slower phase the Voc and ff continue to increase while the isc decreases. The overall efficiency still increases noticeably reaching an unprecedented 11.2 percent after 600 –900 hours. The second phase probably reflects adsorption of water at the interface shifting the conduction band of the oxide to a higher level.

3.12 Tandem Devices:

In the beginning of this report, we have mentioned about the tandem cell concept, by which we wanted to attain higher efficiencies in solar energy conversion. For checking the proof of the tandem device concept, first such a trial device is fabricated. Since the organic dye synthesis was still underway at that time, a tandem cell was constituted using a normal dye sensitized solar cell and a thin layer CdTe bottom cell, which absorbs IR wavelengths similar to the above dyes. IPCE measurements of the CdTe device alone indicates that about 10 – 20% increment over the 11.2% efficiency figures reported for the DSC alone is attainable by the extended light absorption.

Figure 35 shows the individual IPCE (incident photons to current conversion efficiency) spectrum of the dye sensitized solar cell (DSC) and the CdTe back cell (which could be replaced by another DSC if and when an IR sensitive dye is available for testing). Combined, the two cells envelope the spectral region ranging from 400 to 850nm. The tandem cell has been constructed using a refractive index matching fluid, with a refractive index = 1.52. The data from the tandem device is shown in figure 36.

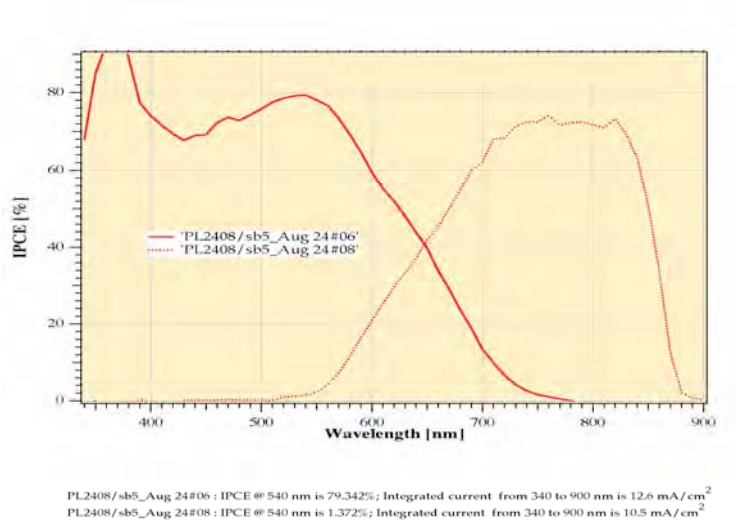

Figure 35: Individual IPCE spectra of DSC (bold line) and CdTe (dotted line). The DSC is made with 10μm TiO_2 film on ITO glass

It is worth noting that such a device would be good for both low level and high light level conditions. The total estimated current from the IPCE data amounts to 24 mA/cm^2, which is sufficient for obtaining about 12% efficiency under AM 1.5 sunlight. The individual currents for the DSC and CdTe were 12.6 and 10.5 mA/cm^2, respectively, as shown in figure 35. In the combined cell, the light through the spectral window between 600 to 700nm is effectively harvested.

Finally, figures 37 and 38 show I-V curves of a tandem device connected in parallel. Figure 37 shows the IV data of the cell made out of 9 microns thick layer TiO2 with Ru dye. Figure 38 shows the total I-V of the tandem device with the CdTe cell. At this stage, the intention is to replace the CdTe cell with a suitable dye cell as soon as a dimensionally correct cell with the longer wavelength absorbing organic dye is fabricated. The thin layer front cell measures 8.07% conversion efficiency and together with the CdTe cell in tandem, the registered output is 12.08%.

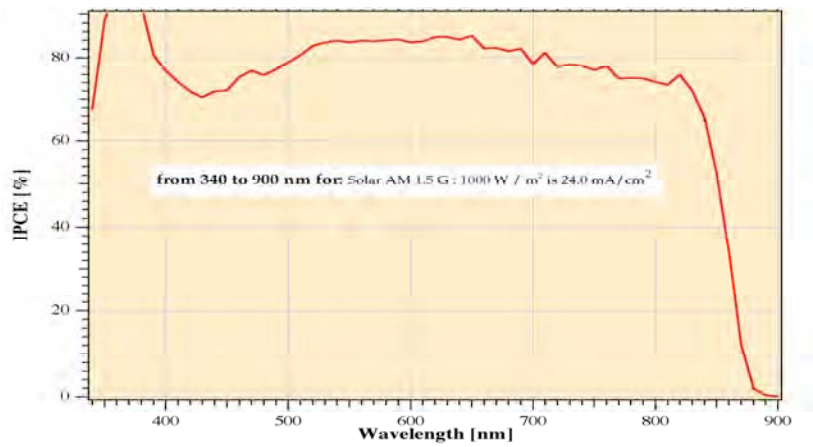

Figure 36: Total IPCE spectrum of the tandem device. DSC is placed in front and the CdTe cell is at the rear. A refractive index matching fluid is applied in-between the cells

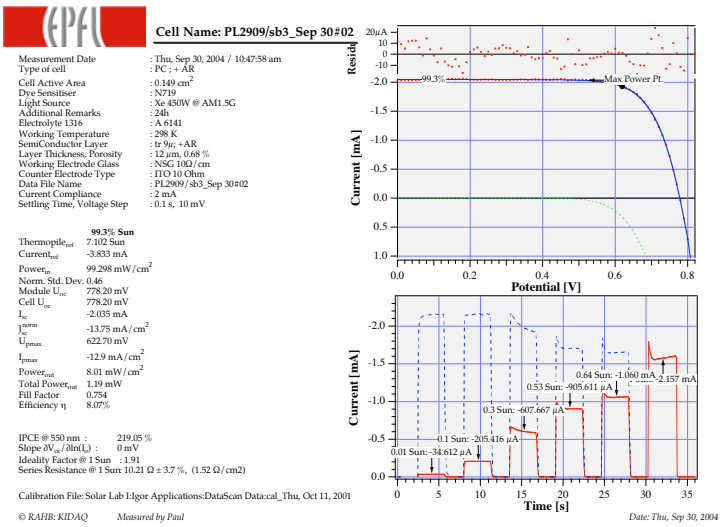

Figure 37. IV curve of a Ru cell (TiO2 layer = 9 microns; to make it thin enough for allowing transmittance of linger wavelengths for absorption by the cell placed behind)

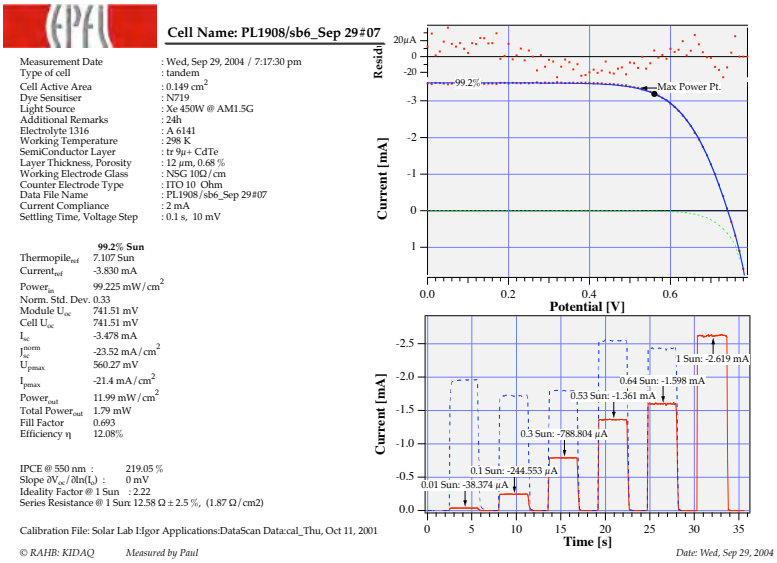

Figure 38. IV curve of the two cells in tandem (connected in parallel); Conversion efficiency is 12.08%

3.13 Finalizing the top cell configuration of the tandem device:

After demonstrating the proof of concept, it is necessary to fabricate an efficient tandem cell, which can harvest both the visible and the near –IR wavelengths of the solar spectrum. In order to be effective, the top cell configuration should be such that it achieves at least 8% conversion efficiency using a dye sensitized mesoscopic TiO_2 film that is transparent in the wavelength domain above 700-750 nm. After extensive screening work, the heteroleptic ruthenium dye K-19 was shown to be the most suitable sensiitzer for the top layer cell.

The advantage of K-19 is that its extinction coefficient is 50% higher than the analogue Z-907, while maintaining an excellent stability when used in conjunction with ROBUST, a nonvolatile electrolyte based on a mixture of n-propyl-methylimidazolium iodide, methoxypropionitrile, N-methylbenzimidazol and guanidinium thiocyanate. Deviations in conversion efficiency are less than 2% when this top cell is subjected to 1000 hours of thermal stress at 80 °C and 1000 hours of light soaking at 60 °C in an air mass 1.5 solar simulator. Typical stability data are shown in Figures 39 and 40. Further to this data set, we have improved the open circuit cell voltage to 800 mV, by using this dye.

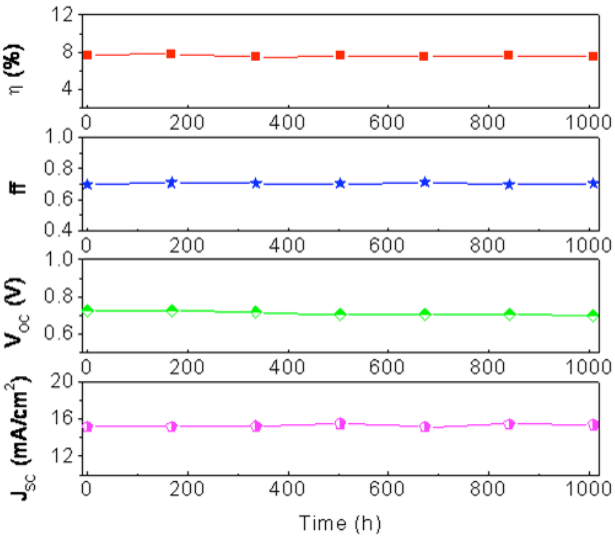

Figure 39. Stability of photovoltaic device parameters of a top layer cell based on K-19 sensitizer and ROBUST electrolyte under thermal stress at 80 °C.

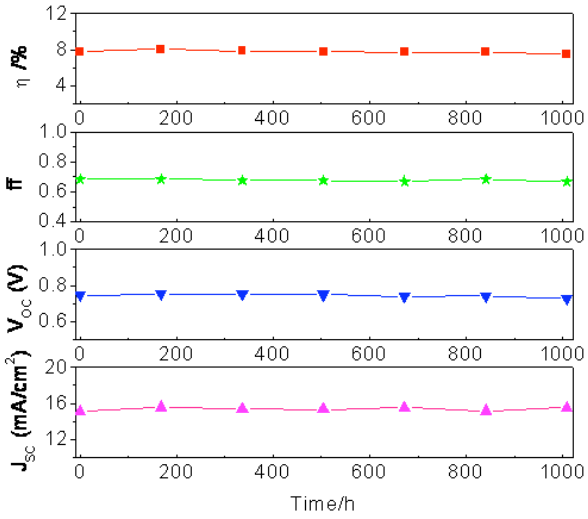

Figure 40. Stability of photovoltaic device parameters of a top layer cell based on K-19 sensitizer and ROBUST electrolyte under light soaking at 1000 Watt/m^2 and 60 °C.

As mentioned earlier, the top cell performance is critical for the overall efficiency of the tandem structure. It should have a conversion yield of over 8% while maintaining excellent transparency in the red and near IR region of the solar spectrum. Figure 41 below shows a transmission spectrum of the mesosocopic TiO_2 film used as top electrode of tandem cell and loaded with K-19 dye.

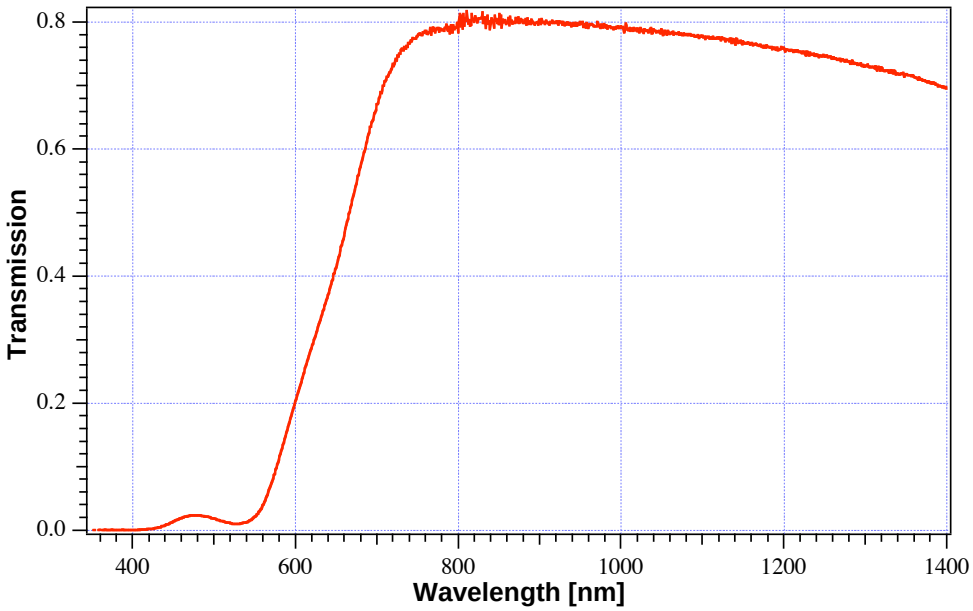

Figure 41. Transmission spectrum of the mesoscopic TiO_2 film derivatized with K-19 dye use as a top electrode in the high efficiency tandem cell.

Figure 41 illustrates that a strikingly high transparency can be reached with the top cell exceeding 70% over a wide wavelength range covering the red and near IR region of the spectrum. This forebodes well for the use of such an electrode in the high efficiency tandem cells. In actual cell measurements, the efficiency of such a transparent sensitized TiO_2 film was impressively high reaching 8.3%.

3. 14 Work on the bottom cell:

The bottom cell will be in series connected to the top cell. In such a configuration it has to generate at least the same photocurrent as the top cell (10- 16 mA/cm^2) using the solar light that passes through the top layer, i.e. photons with longer wavelength than 700 -750 nm. In one embodiment, we want to employ a thin layer of CIGS (cupper indium gallium selenide) as the bottom cell. The onset of the photocurrent for CIS is at 1230 nm and the cell delivers an open circuit voltage of 0.55 V. The CIS cell generates a short circuit photocurrent of ca 36 mA/cm2 of which more than half arises from wavelength above 700 nm. Hence the 15 mA/cm2 generated in the top cell will be readily sustained by the CIS bottom layer. In series connection of the two systems will produce an open circuit voltage of at least 1.35 V. For obtaining a15% conversion efficiency, a fill factor of 0.74 is required, which is within reach.

This strategy has been experimented and the actual result is shown in Figure 42.

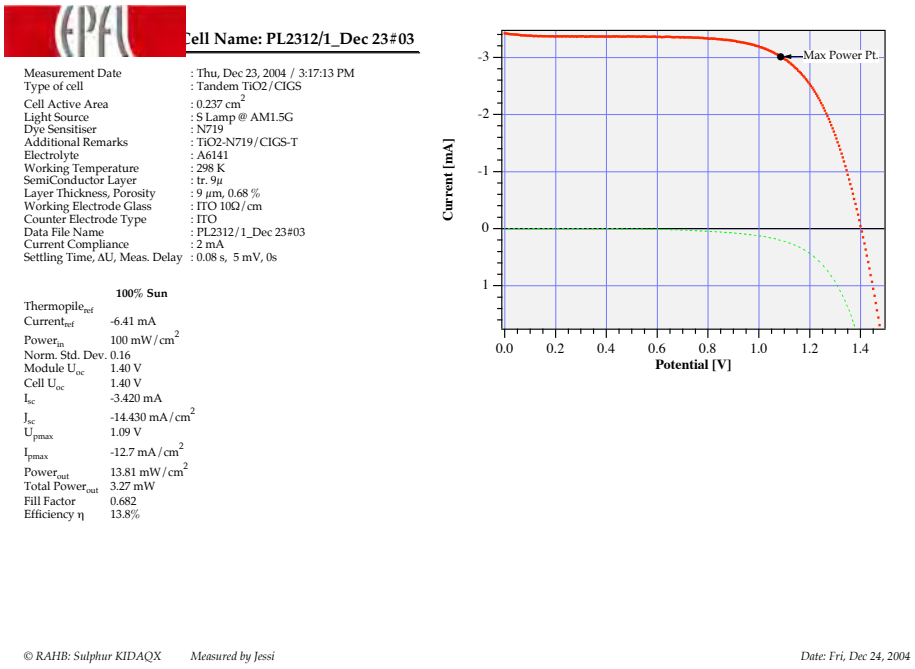

Figure 42. IV data of the tandem device showing 13.8% conversion efficiency at 1.5 AM white light.

The first tandem cell arranged in this manner showed a conversion efficiency of 13.8% at AM 1.5 simulated sunlight. The fill factor was lesser than expected (0.682 vs 0.74), due to certain contact problems. This is rectifiable and we moved on with the idea.

3.15 Work on the complete tandem cell:

EPFL then implemented a full tandem cell configuration, which has produced striking improvements in the conversion efficiencies. Shown in Figure 43 is an example for the spectral response of the photocurrent of the two separate cells and the tandem device. The tandem device achieves a very high external quantum efficiency (EQE) of about 80 percent in the entire visible and near IR range.

A double junction cell of this type attained a conversion efficiency of 15% under standard global AM 1.5 sunlight illumination. A photocurrent voltage curve illustrating the performance of such a cell is shown in Figure 44.

After having reached 15% conversion efficiency we started to look at the idea of building a tandem device, whose structure is shown in Figure 45. This embodiment has a good chance to achieve the efficiency target. This configuration is advantageous for the case, where the top cell is unable to support the high photocurrents produced by the bottom cell due to its extended IR wavelength response. This particular embodiment is designed to yield an open circuit voltage of 2.2 V at a short circuit photocurrent density of 12 mA/cm^2. With a realistic fill factor of 0.76 the device will give 20% efficiency.

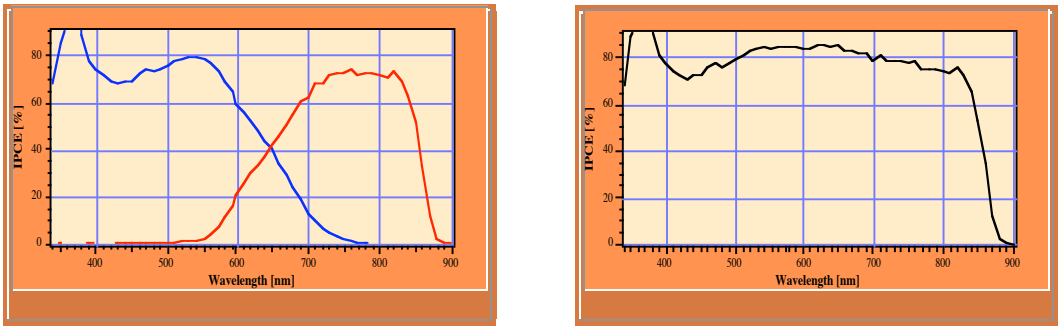

Figure 43. (Left side): spectral response curves of the photocurrent for a DSC top electrode (blue line) and a red and near IR sensitive bottom cell (red line). The external quantum efficiency (incident photon to current conversion efficiency) is plotted as a function of wavelength of the incident light; (Right side): spectral response of the tandem cell

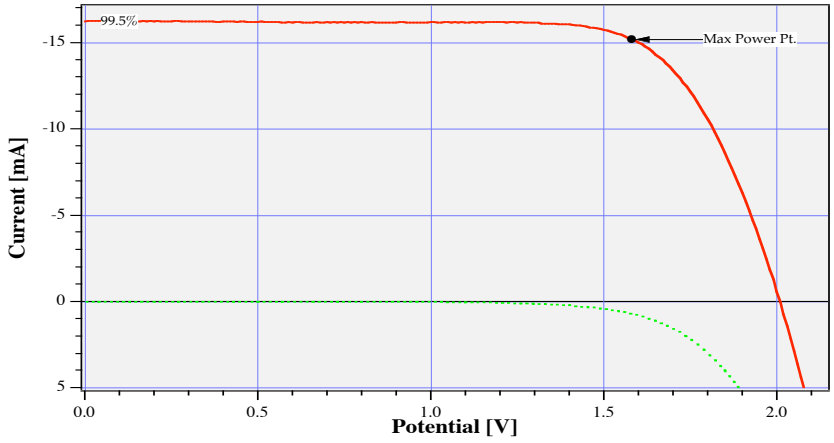

Figure 44. I-V curve of a tandem cell using a DSC as top electrode. The device size is 1.6 cm^2. Values for Isc, Voc, ff and the overall efficiency are 10.16 mA/cm2, 2.01 V, 0.737 and 15.05%, respectively.

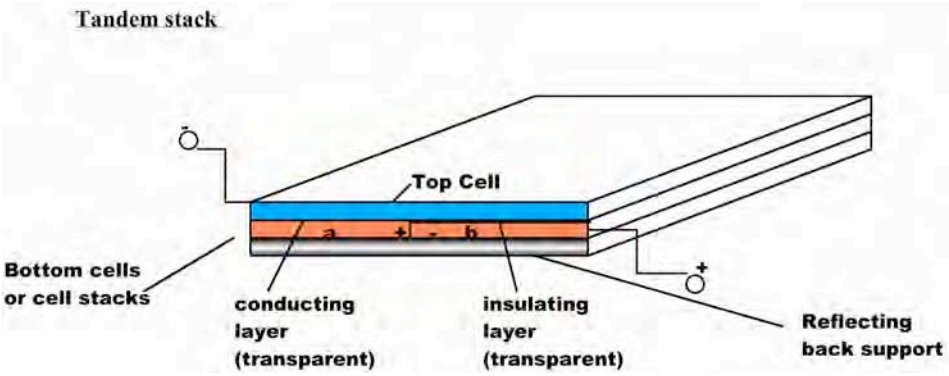

Figure 45. *Tandem Cell concept showing a visible light absorbing top DSC (1) with 2 bottom cells (a & b) absorbing IR wavelengths, all in series connected. The tandem cell is expected to generate a Voc of 2.2 V. The short circuit current will be around 12 mA/cm^2 and the fill factor at least 0.76. The total conversion efficiency yield will reach ≥20%.*

In such a device, where the top cell is always a DSC, we will have several options for the bottom cell: (1) an n-p junction, (2) a Q-dot sensitized TiO2 based cell, where the Q-dot is able to perform FRET (fluorescent resonant energy transfer) and (3) DSC containing an organic dye capable of absorbing IR wavelengths.

The top cell performance is critical for the overall efficiency. It should have a photocurrent of 12 mA/cm2 and a voltage of 1 V. Already by April 2005, we have achieved an open circuit voltages around 0.8 V. The approach to reach higher Voc values was to reduce the dark current of the cell. Thus decreasing the dark current by a factor of 100 will produce the wanted 180 mV gain in open circuit voltage. The strategies we pursued to suppress the dark current are:

i) To decrease the film thickness by employing organic dyes with higher extinction coefficients.
ii) To deposit by atomic layer deposition (ALD) a 1 nm thick film of an insulator in a conformal manner.
iii) To use additives as co-adsorbents that would enhance the Voc.

We have already observed the benefits of i) and iii). A striking augmentation of the Voc was discovered when guanidinium butyric acid (GBA) was used as a co-adsorbent along with an amphiphilic ruthenium sensitizer.

Significant improvements in Voc and Isc in DSC have been achieved during June 2005. By using a combination of Z-907 dye and GBA co-adsorbent along with the robust electrolyte, we have measured the following cell characteristics.

Cell Parameters	**DSC used in Tandem Cell in March '05**	**New DSC**
Voc, (V)	0.84	0.883
Isc (mA/cm^2)	10.2	10.52
Fill Factor (FF)	0.737	0.65

The reason for the observed lower fill factor pertains to the type of conducting glass used in this new experiment. It was made on ITO, instead of fluorine doped tin oxide and the TiO_2 electrode heat processing caused higher sheet resistivity. Therefore, if we take the same FF, as measured with tin oxide glass, then the combined tandem device's (top cell + bottom cell) OCV and Isc will be 2.053 V and 10.52 mA/cm^2, respectively. Using 0.737 as FF, the total conversion efficiency is 15.9%.

The top cell performance is critical for the overall efficiency. To reach the efficiency target of 20 percent it should have a photocurrent of 12 mA/cm2 and a voltage of close to 1.0 V. So far we have achieved open circuit voltages around 0.88 V. The approach to reach higher Voc values is to reduce the dark current of the cell. In order to understand the dark current problems, a detailed analysis was performed employing electrochemical impedance spectroscopy and transient photo voltage decay methods. Additionally, photocurrent-voltage characteristics, dark current and cyclic voltammetry were also carried out.

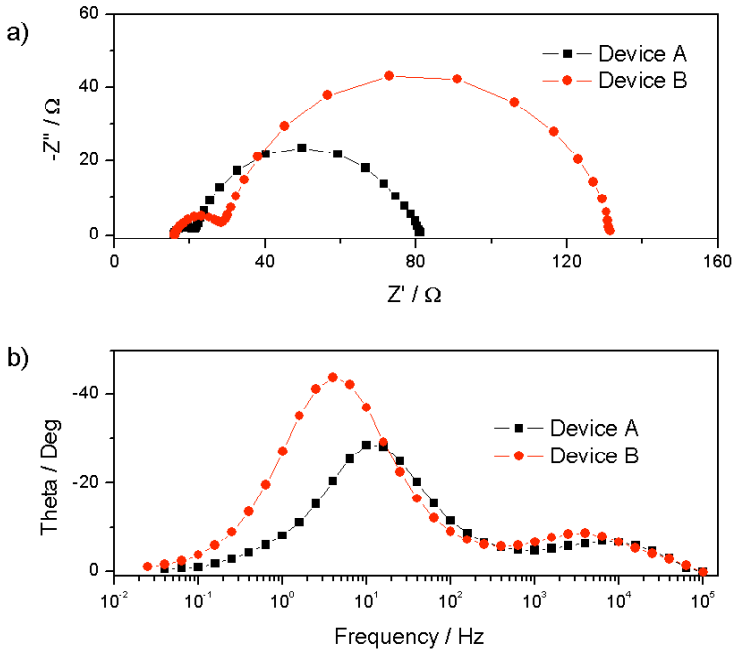

Figure 46. Typical electrochemical impedance spectra of device A (self-assmbled amphihpilic sensitizer alone) and B (mixed self-assembled monolayer containing amhpiphilic sensitizer and GBA) in the form of a) Nyquist plots and b) Bode plots. The spectra were measured with an external potential of -0.72V in the dark.

Figure 46 shows typical electrochemical impedance plots obtained from DSC in the absence (A) and presence (B) of GBA co-adsorbed with the sensitizer at the mesoscopic TiO2 electrode surface. The co-adsorption of GBA produces a pronounced increase in the radius of the hemi-circle in the Nyquist plot and the shift of the phase angle to lower frequencies in the Bode plot. The results indicate that GBA shifted the conduction band of TiO_2 towards a more negative potential and reduced the interfacial charge transfer reaction from conduction band electrons to

triiodide in the electrolyte (also known as the back reaction). In addition, the devices with GBA co-grafting showed an excellent photo-stability, as discussed earlier.

The use of GBA as a co-adsorbent along with the amphiphilic sensitizer, allowed the increase of the Voc from 0.84 to 0.883 V, and the short circuit photocurrent from 10.2 to 10.52 mA/cm^2. The replacement of the ITO by an FTO counter electrode has permitted to eliminate the fill factor loss mentioned before and allowed for the first time 16% conversion efficiency in the full tandem cell.

3.16 Work on the integral tandem cell:

This work focuses on the development of conducting transparent interconnects acting as recombination layers. This will minimize optical losses in the stack and the work is progressing.

We continued also our research on quantum dots of II-IV semiconductors as light harvesting units. PbS quantum dots have been synthesized and attached to the mesoscopic TiO2 film by a thioacetic acid linker. We are also very excited about our observation of exciton transfer by FRET (Foerster resonance Energy transfer) from quantum dots to surface adsorbed charge transfer sensitizers. This shows that the quantum dot can be employed as a light harvesting antennae opening up new possibilities for improving the efficiency of mesoscopic solar cell.

Further we are working on the development of conducting transparent interconnects acting as recombination layers. This will minimize optical losses in the stack. Finally we started to implement a simplified embodiment of the on tandem cell where the bottom layer is integral and not split in two in series connected individual cells as used so far. Cells of this type are easier to scale up and to produce industrially. The maximum conversion efficiency that can be reached with such a configuration is about 46% as shown in Figure 47.

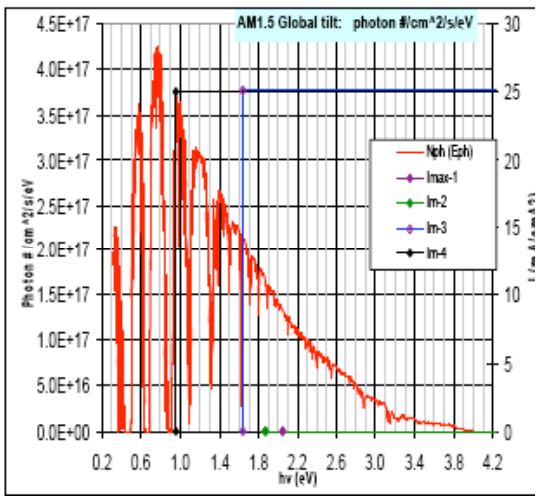

Figure 47. AM 1.5 global solar emission spectrum and optimal band gaps for the top and at top and bottom cells of the DSC at 1.65 and 1 eV. The photocurrent is matched at 25 mA/cm2 yielding an overall conversion efficiency of 46 percent

3.17 Losses in the tandem device:

After having attained 16% conversion efficiency, our work focused on identifying the main loss factors in the tandem cell embodiment whose elimination will lead to a further boost in the conversion yield. By the end of 2005, we were consolidating the important output of the several months' work on tandem cells and soon after published a paper in Applied Physics Letters. During this period, many experiments, particularly on the transparency of various types of conducting glasses, have been carried out. We have now simplified the embodiment of the tandem by using a single CIGS cell as the bottom cell. This configuration will facilitate to reach the efficiency target of at least 20% in the short-to-medium term besides being easier to produce than the earlier configuration, where the bottom cell was constituted by two series connected CIGS cells. The roadmap to reach the 20% conversion efficiency is straightforward: besides matching the photocurrents of the two cells more closely as is evident from our work, the increased transparency of ITO in the near IR regions also can be exploited beneficially. The absorption of light by the CIGS bottom cell extends up to 1180 nm, which is clearly in the spectral domain where the FTO electrode used for the top cell has a significant light absorption. Therefore in the stacked configuration, this near IR light absorption by the FTO collector electrode in the DSC top cell leads to a loss of the photocurrent in the bottom cell and hence a reduction of overall efficiency. The future effort should be particularly directed towards eliminating this problem and to replace FTO with ITO. For this to be effectively realized, we have to improve the surface adhesion of TiO_2 onto ITO. Several procedures including PVD methods (including magnetron sputtering of a compact TiO_2 under-layer) are good options for successfully meeting this challenge.

3.18 Improvement of the near-IR transmission of top cell:

As stated in the previous paragraphs, the optical loss could be reduced significantly by using ITO instead of FTO on glass. We discovered also that if ITO glass is briefly treated in air at 500 °C, its transmission in the near IR increases drastically while maintaining an acceptable sheet resistance of 15 ohm/square. This is expected to give a boost in overall conversion efficiency.

3.19 Optimization and matching the I-V characteristics of the top and bottom cells:

In addition to the modifications desired on the transparency of the top cell, which are dependent on the materials chosen, improvements in the tandem device performance could be possible by further optimizing the voltage and current characteristics of the two individual cells. An increase in voltage adds to the total output voltage of the tandem device. On the other hand, the current produced by the two cells should match one another to produce an optimized total output. Though the current output of CIGS is higher than DSC, its open circuit voltage (OCV) is relatively lower. Since a current matching is anyway required (usually to lower values) between the two cells, we have some room for augmenting the OCV of the DSC by judiciously playing with the TiO_2 layer thickness and other chemical modifications. Therefore, cells were made by keeping the layer thickness at 8 microns, but were modified by an additional $TiCl_4$ thermal treatment before adsorbing the dye.

It is true that for controlling the transmittance of light across the top cell, the thickness of TiO_2 layer will have to be altered. However, if it is brought down substantially, then the current density of DSC will have to be compromised due to insufficient light absorption by the dyed TiO_2 layer. This problem could be solved, by using dyes showing relatively higher extinction coefficients when compared to the Ru dye. Organic dyes are appropriate for this purpose. We have recently identified an indoline dye, which caters to this purpose. The indoline dye employed is referred to as "D149" and it shows a 5-times higher extinction coefficient (68700 mol^{-1} cm^{-1} at 526 nm) compared to the conventional Ru dye (N719: 13900 mol^{-1} cm^{-1} at 541 nm). Figure 48 shows the IPCE spectrum of a DSC measured using this new dye. The data clearly indicates that D149 shows a threshold of absorption starting from 750nm onwards, rising sharply and covering almost all photons up to 400nm. Figure 49 shows the dye structure.

Work in our laboratory using D-149 had revealed that, a high current density is achievable by using a very thin layer of TiO_2, due to the desired visible absorption spectrum and the high extinction coefficient. Figure 3 shows that by using just 3 – 4 microns thick TiO2 layers, short circuit current densities >16 mA/cm^2 could be obtained.

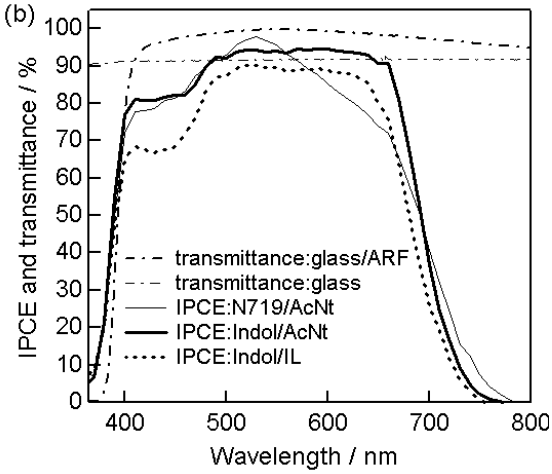

Figure 48. Transmittance of a glass plate with/without anti-reflecting film (ARF), and IPCE spectra of DSC with the indoline dye in the presence of two types of electrolytes (AcCN and IL). Data for cells with N719 (Ru-dye) and AcCN electrolyte is also shown. The IPCE spectrum of D149/IL was corrected for the non-linearity in the irradiation intensity.

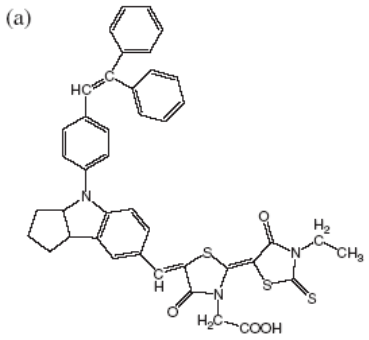

Figure 49. Structure of D-149

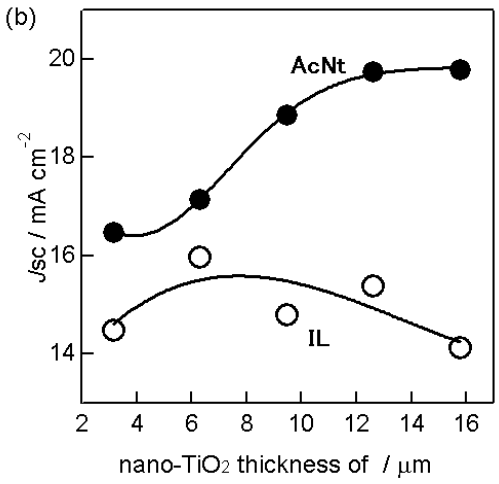

Figure 50. Short circuit current densities obtained from D-149-sensitized solar cells using AcCN and IL electrolyte as a function of nanocrstalline TiO_2 film thickness.

3.20 New Tandem Cell containing DSC With Record Output:

We have fabricated a new tandem device, containing a DSC as the top cell and a CIGS cell as the bottom cell. The output of this tandem device is higher than what we have demonstrated in 2005 (and reported in *Applied Physics Letters* ***88****, 203103 (2006)*). Compared to the 15.75 % combined conversion efficiency by four-wires measurement, demonstrated in 2005 work involving DSC and CIGS, we have now reached 16.1% efficiency. Against the 15.09% efficiency reported then by doing a 2-wires measurement, we now have 15.76%. This improvement is the result of our effort in increasing the performance of the top DSC, reducing the optical losses arising out of FTO glass, optimization of the transmitted light from DSC to CIGS, and better current matching of the two cells. The top DSC now produces 8.6% efficiency, compared to the 8.1% achieved earlier. Figures 51 – 53 show the relevant data. In the top DSC, the light absorbing electrode is made of FTO (NSG 10 ohm; 4mm thick), but the counter electrode is made of ITO. During this experiment, we have identified

one more loss factor. This arises out of the step involving chemical deposition of Pt catalyst on the counter electrode. This chemical procedure, though is harmless with FTO glass, causes the ITO glass to increase its electrical resistance by at least 20 ohms/square. Our next effort is to sputter Pt and avoid the chemical treatment. We expect that sputtered Pt will reduce the electrical resistivity of DSC further, and the overall cell efficiency elevate to further higher values.

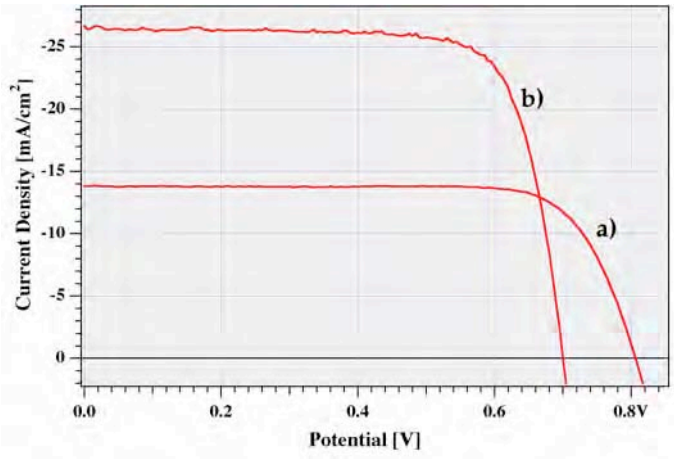

Figure 51. Separately measured DSC and CIGS cells. a) DSC measured under AM 1.5 sunlight giving 8.63% efficiency; b) CIGS measured under similar irradiance, giving 14.11 % efficiency.

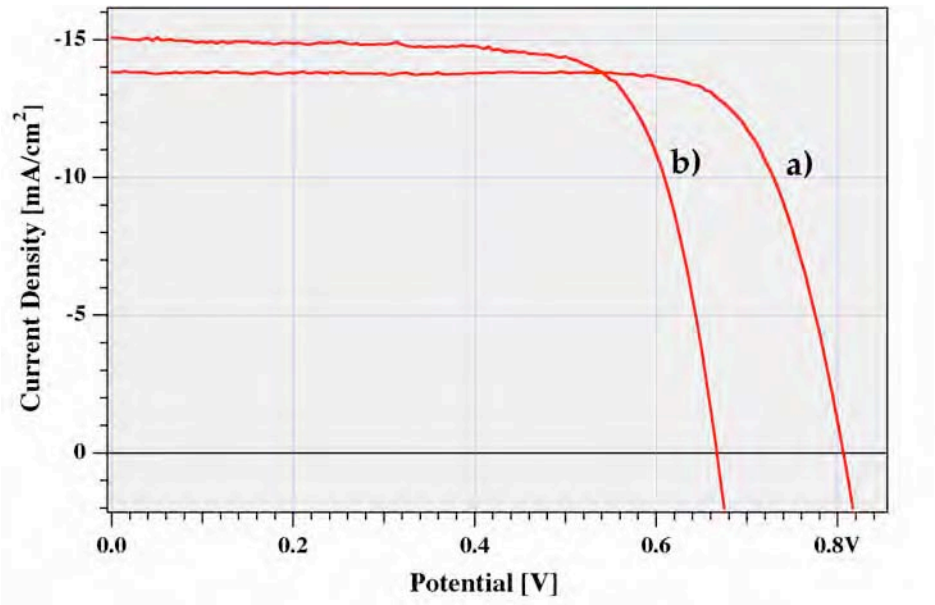

Figure 52. Tandem device output in 4 wires measuring mode under AM 1.5 sunlight. The top DSC gave 8.63% and the bottom CIGS gives 7.47% efficiencies. Hence the combined output is 16.1%, in 4-wires mode.

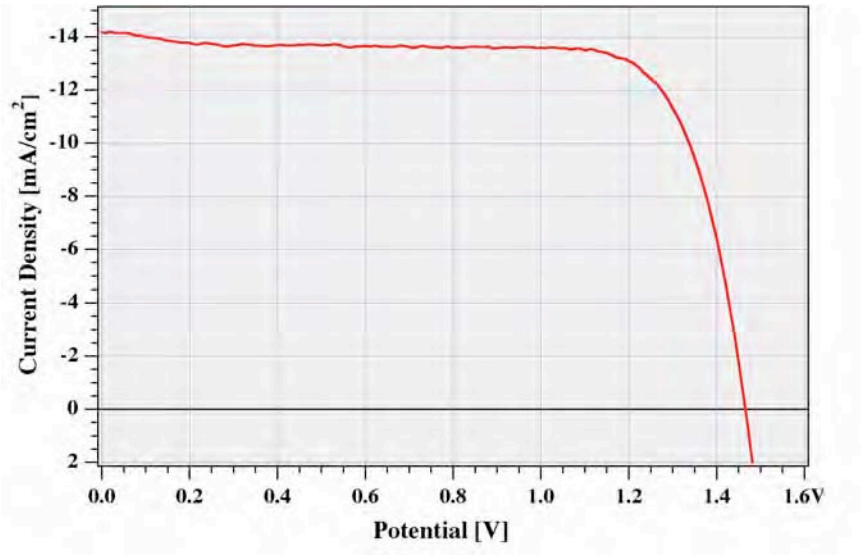

Figure 53. The tandem device in 2-wires measuring mode under AM 1.5 sunlight. The cell output shows 15.76% efficiency.

4. Conclusions

During this project period, we have demonstrated a new type of tandem cell consisting of a top DSC and a bottom CIGS cell. The DSC by itself can now show > 11% conversion efficiency. The measured efficiencies of the tandem device in 4 wires mode and 2-wires mode are 16.1% and 15.75%, respectively. Further improvements are possible on the tandem device by decreasing the losses in ITO and FTO conducting glasses. Several new organic and inorganic dyes absorbing extended red and IR regions have been synthesized. Though not all these dyes perform well in DSC as desired, they have indeed opened up newer possibilities. Thus Ru-free substitutes for the top-DSC also have been identified and a very promising near-IR dye based on a triaryl substituted cyanine has been synthesized. The project has produced several new high quality publications.

5. List of Publications under this project:

1. ‘Efficient Light Harvesting by Using Green Zn-Porphyrin-Sensitized Nanocrystalline TiO2 Films’ Q. Wang, W.M. Campbell, E.E. Bonfantini, K.W. Jolley, D.L. Officer, P.J. Walsh, K. Gordon, R. Humphry-Baker, Md.K. Nazeeruddin, M. Grätzel, J. Phys. Chem. B 109, 15397-15409 (2005).

2. ‘Organized Mesoporous TiO2 Films Exhibiting Greatly Enhanced Performance in Dye-Sensitized Solar Cells’, M. Zukalova, A. Zukal, L. Kavan, Md. K. Nazeeruddin, P. Liska, M. Grätzel, Nano Letters, Vol. 5, No. 9, 1789-1792 (2005).

3. ‘Synthesis of novel ruthenium sensitizers and their application in dye-sensitized solar cells’, Md. K. Nazeeruddin, C. Klein, P. Liska, M. Grätzel Coordination Chemistry Reviews 249, 1460-1467 (2005).

4. 'Charge Separation and Efficient Light Energy Conversion in Sensitized Mesoscopic Solar Cells Based on Binary Ionic Liquids', P. Wang, B. Wenger, R. Humphry-Baker, J.-E. Moser, J. Teuscher, W. Kantlehner, J. Mezger, E. V. Stoyanov, S.M. Zakeeruddin, M. Grätzel, J. Am. Chem. Soc., 127, 6850-6856 (2005).

5. 'Zn-Porphyrin-Sensitized Nanocrystalline TiO2 Heterojunction Photovoltaic Cells', L. Schmidt-Mende, W.M. Campbell, Q. Wang, K.W. Jolley, D.L. Officeer, Md.K. Nazeeruddin, M. Grätzel, ChemPhysChem 6, 1253-1258 (2005).

6. 'Dye-Sensitized Solid-State Heterojunction Solar Cells', M. Grätzel MRS Bulletin, Vol. 30. 23-27 (2005).

7. 'Engineering of a Novel Ruthenium Sensitizer and Its Application in Dye-Sensitized Solar Cells for Conversion of Sunlight into Electricity', C. Klein, Md.K. Nazeeruddin, P. Liska, D. Di Censo, N. Hirata, E. Palomares, J.R. Durrant, M. Grätzel, ,Inorg. Chem. 44, 178-180 (2005).

8. 'A High Molar Extinction Coefficient Sensitizer for Stable Dye-Sensitized Solar Cells', P. Wang, C. Klein, R. Humphry-Baker, S.M. Zakeeruddin, M. Grätzel, J. Am. Chem. Soc. 127, 808-809 (2005).

9. 'Efficiency improvement in solid-state-dye-sensitized photovoltaics with an amphiphilic Ruthenium-dye', L. Schmidt-Mende, S.M. Zakeeruddin, M. Grätzel, Appl. Physics Letters 86, 013504-1-013504-3 (2005).

10. 'Stable new Sensitizer with Improved Light Harvesting for Nanocrystalline Dye-Sensitized Solar Cells', P. Wang, S.M. Zakeeruddin, J. E. Moser, R. Humphry-Baker, P. Comte, V. Aranyos, A. Hagfeldt, M.K. Nazeeruddin, M. Grätzel, Adv. Mater. 16, No. 20, 1806-1811 (2004).

11. 'Synthesis of Novel Ruthenium Sensitizers and their Application in Dye-Sensitized Solar Cell', Md. K. Nazeeruddin, C. Klein, P. Liska and M. Grätzel, Coord. Chem. Rev., 248, 1317-1328 (2005).

12. 'Combined Experimental and DFT-TDDFT Computational Study of Photoelectrochemical Cell Ruthenium Sensitizers', Md. K. Nazeeruddin, Filippo De Angelis, Simona Fantacci, Annabella Selloni, Guido Viscardi, Paul Liska, Seigo Ito, Bessho Takeru and Michael Grätzel, J. Amer. Chem. Soc., 127, 16835-16847 (2005).

13. 'DFT-INDO/S modelling of new high molar extinction coefficient charge transfer sensitizers for solar cell applications', Md. K. Nazeeruddin, Qing Wang, Le Cevey, Viviane Aranyos, Paul Liska, Egbert Figgemeier, Cedric Klein, N. Hirata, James R. Durrant, Anders Hagfeldt, A. B. P. Lever, and Michael Grätzel, Inorg. Chem. 45, 787-797 (2006).

14. 'Recent advances in dye sensitized solar cells', K. Ravindranathan Thampi, P. Liska, P. wang, S.M. Zakeeruddin, L. Schmidt-Mende, C. Klein, P. Comte and

M. Graetzel, Proceedings of the 20th European PV solar energy conference, 2005, WIP-Renewable energies, Munich, Germany, p-55.

15. 'Nanocrystalline dye-sensitized solar cell/copper indium gallium selenide thin-film tandem showing greater than 15% conversion efficiency', P. Liska, K.R. Thampi, M. Graetzel, D. Bremaud, D. Rudmann, H.M. Upadhyaya and A.N. Tiwari, Applied Physics Letters, 88, 203103 (2006).